method for identifying the exact anatomic relation between the sympathectomy target and vessels. Abdominal CT is usually obtained with patients in a supine position. When patients are in a prone position, however, the CT may reveal that the anatomy has shifted. Therefore, CT images obtained in supine patients are not necessarily effective for determining the needle route. In normal anatomy, in most cases the inferior vena cava locates at the right (anterior) side of the vertebra and the aorta locates in the region mid-anterior to the vertebral body, and both major vessels locate more dorsally at the caudal level in the lower abdomen. Although our findings in patients in the prone position were consistent with the normal condition, it might be important to provide numerical anatomic data regarding the location of major vessels for lumbar sympathectomy. Real-time CT fluoroscopic guidance may be more suitable for percutaneous lumbar sympathectomy.

In summary, the present study provides anatomic data regarding major vessels (i.e., vena cava and aorta) in relation to the target of lumbar sympathectomy. The use of CT guidance is recommended for lumbar sympathectomy to reduce the risk of vascular puncture.

Conflict of interest We declare that we have no conflict of interest.

References

1. Breivik H, Cousins MJ (2008) Sympathetic neural blockade of upper and lower extremity. In: Cousins MJ, Carr DB, Horlocker TT, Bridenbaugh PO (eds) Cousins and Bridenbaugh's neural blockade in clinical anesthesia and pain medicine, 4th edn. Lippincott Williams & Wilkins, Philadelphia, pp 848–885
2. Curatolo M, Bogduk N (2009) Diagnostic and therapeutic nerve blocks. In: Fishman SM, Ballantyne JC, Rathmell JP (eds) Bonica's management of pain, 4th edn. Lippincott Williams & Wilkins, Philadelphia, pp 1401-1423
3. Ryttov N, Boe S, Nielsen H, Jacobsen J (1981) Necrosis of ureter as a complication to chemical lumbar sympathectomy. Report of a case. Acta Chir Scand 147:79–80
4. Redman DR, Robinson PN, Al-Kutoubi MA (1986) Computed tomography guided lumbar sympathectomy. Anaesthesia 41:39–41
5. Kuroda M, Koizuka S, Saito S, Sato E, Takizawa D, Goto F (2005) Computed tomography fluoroscopy-guided lumbar sympathectomy for a patient with peripheral vascular disease and lumbar spine compression fracture. J Anesth 19:268–269
6. Koizuka S, Saito S, Obata H, Tobe M, Koyama Y, Takahashi A (2008) Anatomic analysis of computed tomography images obtained during fluoroscopic computed tomography-guided percutaneous lumbar sympathectomy. J Anesth 22:373–377
7. Tay VK, Fitridge R, Tie ML (2002) Computed tomography fluoroscopy-guided chemical lumbar sympathectomy: simple, safe and effective. Australas Radiol 46:163–166
8. Koizuka S, Saito S, Kubo K, Tomioka A, Takizawa T, Sakurazawa S, Goto F (2006) Percutaneous radio-frequency mandibular nerve rhizotomy guided by CT fluoroscopy. AJNR Am J Neuroradiol 27:1647–1648
9. Koizuka S, Saito S, Sekimoto K, Tobe K, Obata H, Koyama Y (2009) Percutaneous radio-frequency thermocoagulation of the Gasserian ganglion guided by high-speed real-time CT fluoroscopy. Neuroradiology 27:1647–1648
10. Koizuka S, Saito S, Tobe M, Sekimoto K, Obata H, KoyamaY (2010) Percutaneous radio-frequency mandibular nerve rhizotomy guided by high-speed real-time CT fluoroscopy . Anesth Analg 111:763–767
11. Ohno K, Oshita S (1997) Transdiscal lumbar sympathetic block: a new technique for a chemical sympathectomy. Anesth Analg 85:1312–1316

1521-0111/12/8104-610–619$25.00
MOLECULAR PHARMACOLOGY
Copyright © 2012 The American Society for Pharmacology and Experimental Therapeutics
Mol Pharmacol 81:610–619, 2012

Vol. 81, No. 4
76083/3760320

Impaired Glycinergic Synaptic Transmission and Enhanced Inflammatory Pain in Mice with Reduced Expression of Vesicular GABA Transporter (VGAT)

Makiko Hardy Yamada, Koichi Nishikawa, Kazuhiro Kubo, Yuchio Yanagawa, and Shigeru Saito

Departments of Anesthesiology (M.H.Y., K.K., S.S.) and Genetic and Behavioral Neuroscience (Y.Y.), Gunma University Graduate School of Medicine, Maebashi City, Japan; and Department of Anesthesiology, Wakayama Medical University, Wakayama City, Japan (K.N.)

Received September 26, 2011; accepted January 9, 2012

ABSTRACT

Loading of GABA and glycine into synaptic vesicles via the vesicular GABA transporter (VGAT) is an essential step in inhibitory neurotransmission. As a result of the evidence linking alterations in GABAergic and/or glycinergic neurotransmission to various pain disorders, we investigated the possible influence of down-regulation of VGAT on pain threshold and behavioral responses in mice. The phenotypes of heterozygous VGAT knockout [VGAT(+/−)] mice were compared with wild-type (WT) mice using behavioral assays. In addition, GABAergic and glycinergic miniature inhibitory postsynaptic currents (mIPSCs) were recorded in dorsal horn neurons. Western blot analysis confirmed significant reduction of VGAT protein levels in VGAT(+/−) mice. However, high-performance liquid chromatography revealed that glutamate, GABA, and glycine contents in the whole brain and spinal cord were normal in VGAT(+/−) mice. Behavioral analysis of VGAT(+/−) mice showed unchanged motor coordination, anxiety, memory performance, and anesthetic sensitivity to propofol and ketamine, although thermal nociception and inflammatory pain were enhanced. Patch-clamp recordings revealed that the frequency and amplitude of glycinergic mIPSCs in lamina II neurons were reduced in VGAT(+/−) mice. Genotype differences in glycinergic mIPSCs were more evident during sustained stimulation by solutions with high potassium levels, suggesting that the estimated size of the readily releasable pool of glycine-containing vesicles was reduced in VGAT(+/−) mice. These results provide genetic, behavioral, and electrophysiological evidence that VGAT-mediated inhibitory drive alters very specific forms of sensory processing: those related to pain processing. More close examination will be needed to verify the possibility of VGAT as a new therapeutic target for the treatment of inflammatory pain.

Introduction

GABA and glycine are the primary inhibitory neurotransmitters in the central nervous system (CNS). Glycine mediates synaptic inhibition in the spinal cord, brain stem, and other regions (Lynch, 2004; Betz and Laube, 2006). In the dorsal horn of the spinal cord, nociceptive afferents coming from the periphery make synaptic connections with neurons located in superficial laminae I and II, the first sites of synaptic integration in the pain pathway. Glycinergic and GABAergic inhibition in the spinal cord are known to regulate propagation of nociceptive signals to higher brain regions (Zeilhofer, 2005; Price et al., 2009). In fact, changes in spinal inhibitory neurotransmission have been associated with various pain disorders (Furue et al., 2004). However, investigation of glycinergic inhibitory mechanisms in pain processing has largely focused on postsynaptic glycine receptors (Ahmadi et al., 2002; Harvey et al., 2004); the physiological roles of glycine release machinery from presynaptic terminals have received less attention.

Loading of GABA and glycine into synaptic vesicles via the vesicular transporter is an essential step in inhibitory neu-

This research was supported by the Ministry of Education, Culture, Sports, Science and Technology of Japan [Grant-in-Aid 22791416] (to M.H.Y.), [Grants-in-Aid 20390412, 23659736] (to K.N.), [Grant-in-Aid 21890032] (to K.K.), [Grants-in-Aid 22300105, #23115503] (to Y.Y.); the Japan Medical Association (to K.N.); Japan Science and Technology Agency Core Research for Evolutional Science and Technology; and Takeda Science Foundation (to Y.Y.)

Article, publication date, and citation information can be found at http://molpharm.aspetjournals.org.

http://dx.doi.org/10.1124/mol.111.076083.

ABBREVIATIONS: CNS, central nervous system; VGAT, vesicular GABA transporter; GAD, glutamate decarboxylase; WT, wild type; HPLC, high-performance liquid chromatography; LORR, loss of righting reflex; ACSF, artificial cerebrospinal fluid; IPSC, inhibitory postsynaptic currents; mIPSC, miniature IPSC; HPLC, high-performance liquid chromatography; GlyT, glycine transporter; TTX, tetrodotoxin; RRP, readily releasable pool; GlyR, glycine receptor; PGE2, prostaglandin E2.

rotransmission. Vesicular transporters regulate the uptake and type of neurotransmitter sequestered in synaptic vesicles and, therefore, the amount and type of neurotransmitter released (Masson et al., 1999). Only one vesicular transporter for GABA and glycine has been identified, this having been separately identified by two researchers as a vesicular GABA/glycine transporter (VGAT) (McIntire et al., 1997) and as a vesicular inhibitory amino acid transporter (Sagné et al., 1997). VGAT is expressed mainly in the CNS (McIntire et al., 1997), where it localizes to the synaptic vesicles of GABAergic and glycinergic neurons (Chaudhry et al., 1998; Dumoulin et al., 1999; Takamori et al., 2000). VGAT belongs to a eukaryotic-specific superfamily of H^+-coupled amino acid transporters, and exchanges GABA or glycine for protons. VGAT defines the GABAergic and glycinergic phenotypes of neurons, in addition to the biosynthetic enzymes [glutamate decarboxylase (GAD)] and the plasma membrane transporters (SLC6) of these transmitters (Gasnier, 2004).

This study was performed to elucidate whether genetic manipulation of VGAT would affect behavior, anesthetic sensitivity, and pain thresholds in mice. Unfortunately, VGAT knockout leads to embryonic lethality between embryonic day 18.5 and birth (Wojcik et al., 2006), which prevents us from being able to analyze the influence of complete inactivation of VGAT in the mature CNS. We therefore investigated how down-regulation of VGAT might influence behavioral performance and pain thresholds. Anesthetic sensitivity to intravenous general anesthetics propofol and ketamine were also investigated, because GABA and glycine receptors are potential targets of anesthetic drugs (Nishikawa and MacIver 2000; Mihic et al., 1997; Nishikawa et al., 2002). In this context, we recently reported that *GAD65* gene knockout and the resulting changes in GABAergic inhibition altered anesthetic sensitivity and acute thermal nociception without affecting inflammatory pain (Kubo et al., 2009a,b; Nishikawa et al., 2011). We then investigated how reduced VGAT levels affected GABAergic and glycinergic inhibition in dorsal horn neurons of the spinal cord using patch-clamp methods.

Although GABA mediates fast inhibitory neurotransmission throughout the CNS, glycine acts as an inhibitory neurotransmitter in spatially restricted areas such as the spinal cord, brain stem, and the cerebellum (Lynch, 2004; Betz and Laube, 2006). This spatially more restricted distribution of glycinergic inhibition may be advantageous in situations in which a more localized enhancement of inhibition is needed (i.e., some pain disorders that are caused by diminished inhibition). This is the first study to use genetic, biochemical, behavioral, and electrophysiological approaches to investigate the role of VGAT in behavioral performance including sensory processing. The present study provides evidence that VGAT would be a new potential target for future analgesic drugs, acting via a novel and potentially more selective pathway.

Materials and Methods

Mice

All animal procedures and protocols used in this study were approved by the Animal Care Committee of Gunma University Graduate School of Medicine (protocol 06-47) and performed according to National Institutes of Health guidelines. We generated heterozygous mice lacking exons 2 and 3 on one VGAT allele [VGAT(+/−) mice] (Saito et al., 2010). Adult male wild-type (WT) mice and VGAT(+/−) mice from 12 to 16 weeks old weighing 23 to 28 g were used for behavioral experiments and young male mice from 14 to 21 days old for electrophysiological recordings. Genotypes were determined by polymerase chain reaction, shortly after weaning. VGAT(+/−) mice exhibited no apparent phenotypic abnormalities during development and adulthood. Mice were group-housed (four to six per cage) in a pathogen-free transgenic facility (12-h light/dark cycle, room temperature 27 ± 2°C), and water and food were available ad libitum. The behavioral studies were performed by a single experimenter who was blinded to the genotypes of the mice. Mice were kept warm by a heat lamp before and throughout the behavioral experiments to avoid hypothermia. None of the animals were used for more than two experiments and at least 1 week was allowed between the two treatments for the mice to recover.

Western Blot Analysis

VGAT(+/−) mice and WT mice at 12 weeks old were decapitated under anesthesia, and the whole brain or spinal cord was rapidly dissected and homogenized in ice-cold homogenization buffer (320 mM sucrose, 50 mM Tris-HCl, pH 7.2, 5 mM EDTA, and 1 mM PMSF). Homogenates were centrifuged at 3000 rpm for 10 min at 4°C to obtain the supernatant. The protein concentrations were determined by BCA protein assay reagent (Thermo Fisher Scientific, Waltham, MA) with bovine serum albumin as a standard. Equal amounts of proteins were separated by 7% SDS-polyacrylamide gel electrophoresis for detection of VGAT and β-actin. The proteins were transferred onto nitrocellulose membranes using a semidry transfer method. After blocking for 1 h with 5% nonfat milk in Tris-buffered saline plus 0.1% Tween 20, the trans-blots were reacted with rabbit anti-VGAT antibody (1:1000; Takamori et al., 2000), or mouse anti-β-actin antibody (1:10,000; Abcam, Cambridge, UK), followed by reaction with secondary anti-rabbit horseradish peroxidase or anti-mouse horseradish peroxidase. Peroxidase activity was detected visually by chemiluminescence using Western Blotting Analysis System (GE Healthcare, Chalfont St. Giles, Buckinghamshire, UK) and imaged by light capture (ATTO, Tokyo, Japan). For quantification of the protein levels, the images were scanned by Scion Image software (Scion Corporation, Frederick, MD).

Measurement of Neurotransmitter Content

For analysis of neurotransmitter tissue content, WT mice and VGAT(+/−) mice at 12 weeks of age were sacrificed by decapitation under deep isoflurane anesthesia. Tissue samples of the whole brain and the whole spinal cord were removed quickly, and tissue weight was measured. The tissue was added to 3 to 5 ml of saline (saline volume was approximately 10 times tissue weight) and then homogenized in phosphate-buffered saline containing 0.2% protease inhibitor using a homogenizer (24,000 rpm, 15 s, 2–3 times; Polytron; Kinematica, Littau-Lucerne, Switzerland). After removal of cell debris by centrifugation at 3000 rpm (20 min, 4°C), the supernatant (500 μl), which was added to sulfosalicylic acid (750 μl), was centrifuged again at 3000 rpm (20 min, 4°C). The supernatant after pH adjustment was analyzed using high-performance liquid chromatography (HPLC) and fluorescence detection. HPLC was performed by SRL (Tokyo, Japan). Neurotransmitter content (nanomoles per gram) was calculated as follows: measured neurotransmitter concentration (nanomoles per milliliter) × saline volume added (milliliters)/tissue weight (grams).

Behavioral Assays

Hotplate Test. An animal was placed on an aluminum plate (25 × 20 cm) maintained at 53 ± 0.5°C, and a Plexiglas cage (24 cm in height) was used to restrict the movements of the animal [hot plate analgesia meter (MK-350C; Muromachi Kikai Co., Ltd, Tokyo, Japan)]. Mice remained on the plate until they performed a behavior indicative of nociception: hind-paw licking and/or jumping. The latency to responses was measured. Only hind-paw responses were

used, because forepaw responses are components of normal grooming behavior. To prevent tissue damage, the cut-off latency was set at 60 s in control experiments or 80 s in drug-treated experiments. Animals not responding within the cut-off time were removed and assigned a score of the cut-off time. In these experiments, mice did not show any behavior to conclude that they had been injured in any way. All measurements were carried out between 6:00 PM and 10:00 PM.

Tail-Immersion Test. The spinally mediated nociceptive thresholds were determined using a thermoregulated water-circulating pump (NTT-20S; Tokyo Rikakikai Co., Ltd, Tokyo, Japan). The mouse was maintained in a mouse holder, and the distal tail was then immersed in the water bath, which was thermostatically controlled at 48 ± 0.5°C. The tail was rapidly immersed in the bath, and the latency to respond to the heat stimulus with vigorous flexion of the tail was measured to the nearest 0.1 s using a manual stopwatch. Animals were removed immediately after responding, and the tail was wiped off with a cloth. The maximum latency allowed was 20 s to prevent tissue damage.

Formalin Test. The test was carried out in individual transparent containers. The mice were placed in the test chambers for 30 min. After this adaptation period, 20 μl of 5% formalin (dissolved in distilled water) was injected into the dorsal surface of the right hind-paw of the mouse, using a 30-gauge needle connected to a microsyringe. Each mouse was returned immediately to the observation place after injection. Animal behaviors after formalin injection were continuously recorded by a video recorder for later analysis. The amount of time the injected hind-paw was lifted, licked, or flinched by the animal was measured for 60 min starting immediately after formalin injection (Dubuisson and Dennis, 1977).

Loss of Righting Reflex. LORR was used as a surrogate measure for general anesthetic hypnosis. Each animal received an intraperitoneal injection of propofol or ketamine and was then placed on its back in a chamber (20 × 28 × 15 cm), and the ability of the mouse to right itself was observed. Mice were judged to have lost this reflex when unable to right themselves within 10 s. The time from intraperitoneal injection of the drug to LORR was considered the latency, and the time between the LORR and the time at which mice regained the ability to right themselves within 2 s was considered the duration of LORR.

Rotarod. To test motor coordination and equilibrium, animals were placed on the rotating RotaRod apparatus (Panlab, S.L., Barcelona, Spain), where the rotational speed of the rod was kept constant at 10 rpm. Mice were trained to remain on the RotaRod until they could perform three consecutive 180-s trials. The latency to fall from the rod was recorded and compared between genotypes.

Open Field Analysis. Spontaneous activity of mice was measured in the Plexiglas transparent open field. Their movements were tracked for 20 min by using an infrared photo-beam detection system for locomotor activity (LE 8811; Panlab, S.L.). This system allowed us to analyze animal trajectories with 16 × 16 infrared beams for optimal subject detection. Behavioral data were stored on a computer for later analysis.

Elevated Plus Maze. Plus-maze test consisted of two open arms (25 × 5 cm, surrounded by a 0.25-cm high border) and two closed arms (25 × 5 cm, surrounded by 15-cm high walls), with the two pairs of identical platform, which emerged from a central platform (5 × 5 cm), positioned opposite each other (EP-3002; Ohara Medical Co., Tokyo, Japan). The apparatus was 50 cm above the floor. Mice were tested on the maze in randomized order. The test was initiated by placing the mouse on the central platform of the maze, facing one of the open arms and letting it move freely. Each session lasted 5 min and was recorded by a video camera. All tests were carried out under dim red lighting between the second and seventh hour of the dark phase. A trained experimenter who was blind to genotype performed behavioral analysis. Several parameters were collected during the session: 1) open arm duration; 2) closed arm duration; 3) central platform duration; 4) open arm frequency; and 5) closed arm frequency.

Morris Water Maze. Spatial memory abilities were examined in the standard hidden-platform acquisition learning versions of the Morris water maze (Schenk and Morris, 1985). A 125-cm diameter circular pool was filled with water kept at 26°C. A 10-cm diameter platform was hidden 1 cm beneath the surface of the water at a fixed position. Mice that failed to find the platform within 60 s were guided to the platform, where they remained for 30 s before being returned to their cages. The mean latency to the platform was recorded.

Patch-Clamp Recordings from Spinal Cord Slice Preparations. The methods of electrophysiology were described previously (Yoshimura and Nishi, 1993; Nishikawa et al., 2011). Slices from young (14–21 days old) male mice were used in this study. In brief, mice were decapitated under deep isoflurane anesthesia, and thoracolumbar laminectomy was performed. The spinal cord at spinal level T12-L1 was removed and then placed in preoxygenated Krebs' solution at 1–3°C. A block of the spinal cord was quickly dissected out and glued to a microslicer tray (DTK-1000; Dosaka EM, Tokyo, Japan) using oxygenated ice-cold modified Ringer's solution. The spinal cord was mounted on a microslicer; a transverse slice (300 μm) was cut from the center of the spinal segment and then kept in the prechamber (Brain Slice Chamber System; Harvard Apparatus, Holliston, MA) filled with artificial cerebrospinal fluid (ACSF) consisting of 125 mM NaCl, 2.5 mM KCl, 2 mM $CaCl_2$, 1 mM $MgCl_2$, 26 mM $NaHCO_3$, 1.25 mM NaH_2PO_4, and 11 mM glucose, bubbled with 95% O_2 and 5% CO_2 at room temperature (22–24°C). Slices were allowed at least 1 h for recovery in the prechamber, which was designed to keep six to eight slices viable for several hours.

Slices were transferred to a recording chamber (2 ml in volume) perfused with an oxygenated ACSF (maintained at 30 ± 1°C; solution heater SH-27A; Warner Instruments, Hamden, CT) at a rate of approximately 6 ml/min. Patch electrodes were made from borosilicate thin-walled capillaries (Harvard Apparatus, Holliston, MA). Recording electrodes (4–6 MΩ) were filled with $CsSO_4$-based solution (110 mM $CsSO_4$, 5 mM TEA,0.5 mM $CaCl_2$, 2 mM $MgCl_2$, 5 mM EGTA, 5 mM HEPES, and 5 mM MgATP, pH 7.2) to investigate spontaneous IPSCs at a holding potential of 0 mV. Whole-cell patch-clamp recordings were made from lamina II neurons using an upright microscope (Axioskop2 FS plus; Zeiss, Jena, Germany). The magnified image was collected by an intensified charge-coupled device camera (Hamamatsu Photonics, Hamamatsu City, Japan) with contrast enhancement. The image of neurons was displayed on a video monitor, and glass patch pipettes were visually advanced using a micromanipulator (MWO3; Narishige Co., Ltd., Tokyo, Japan) through the slice to the surface of the neuron. An Axopatch 200B amplifier (Molecular Devices, Sunnyvale, CA) was used for whole-cell recordings. Whole-cell currents were filtered at 2 to 5 kHz and digitized at 10 kHz (Digidata 1322A; Molecular Devices) and stored on a Pentium-based personal computer. Addition of bicuculline (10 μM; Sigma-Aldrich, St. Louis, MO) or strychnine (300 nM; Sigma-Aldrich) was used to isolate GABAergic and glycinergic IPSCs, respectively. Series resistances were generally between 10 and 25 MΩ and were then compensated approximately 80%.

Data Analysis. Data acquisition and analysis were performed with pCLAMP software version 8.1 (Molecular Devices) and Mini-analysis software (Synaptosoft Inc., Fort Lee, NJ). Synaptic currents were defined as current deflections with a fast rising phase and a relatively slower decay phase. The rise time was defined as time interval between 10 and 90% of the peak amplitude, and synaptic currents having the rise time <2 ms were included for analysis. The amplitude of synaptic current was measured from the initial inflection point (not from the baseline) to the peak, to avoid the effects of summation on amplitude distribution. Threshold-level crossing were set at approximately 3 times baseline noise, which was measured during the period of no detectable events. As a result, synaptic currents larger than 6 pA in the amplitude were counted for analysis. This definition eliminated the infrequently observed single-channel events or synaptic currents with slow rise time but successfully detected most IPSCs. The decay phase was fitted with a single

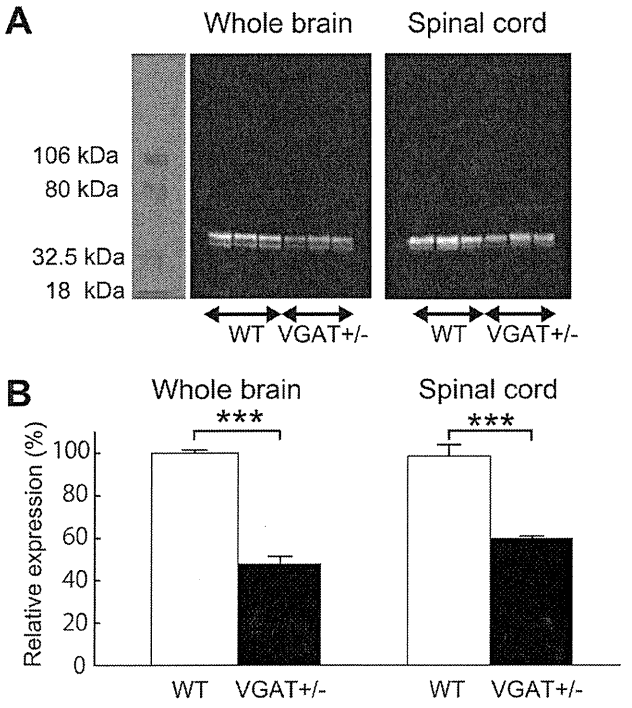

Fig. 1. Abundance of VGAT protein in the whole brain and spinal cord as measured by Western blotting. A, representative immunoblots of VGAT from WT mice and VGAT(+/−) mice. Relative signal intensities were normalized to β-actin. B, results are expressed as percentages of WT values. Data are shown as mean ± S.E.M. (n = 3 each) here and in subsequent figures. ***, $P < 0.001$; **, $P < 0.01$ versus corresponding age-matched WT mice (Student's t test).

exponential curve, and a time from peak to 36.8% of peak was defined as the decay time constant.

Chemicals. For behavioral studies, mice were treated with propofol (Maruishi Pharmaceuticals Co, Ltd., Osaka, Japan) or ketamine (Sankyo Co, Ltd., Tokyo, Japan) administered intraperitoneally with a volume of 10 μl/g of body weight. Vehicle solutions for behavioral studies were as follows: propofol, lipofundin MCT/LCT 10% (B. Braun Melsungen AG, Mulsungen, Germany); ketamine, 0.9% saline. An injection of lipofundin MCT/LCT 10% (10 μl/g i.p.) alone had no hypnotic/analgesic effect on mice behavior (n = 5, data not shown). Other drugs and reagent grade chemicals were purchased from Sigma-Aldrich Chemicals (Tokyo, Japan).

Statistical Analysis. Results are expressed as mean ± S.E.M. The results were analyzed by using Student's t test or one-way analysis of variance. Post hoc comparisons between the individual groups were performed by means of the Tukey test. The level of statistical significance was set at $P < 0.05$ in all tests.

Results

Western Blot Analysis. We first examined the expression of the VGAT protein in WT mice and VGAT(+/−) mice (Fig. 1). The VGAT protein level in the brain from VGAT(+/−) animals was significantly reduced to 47.8 ± 2.1% of WT mice (n = 3, $P < 0.001$). The expression of VGAT in the VGAT(+/−) spinal cord was also reduced to 61.0 ± 0.5% of WT mice (n = 3, $P < 0.01$). These data show that VGAT protein levels are considerably reduced in VGAT(+/−) mice.

GABA and Glycine Levels in the Brain and Spinal Cord Are Normal in VGAT(+/−) Mice. We measured neurotransmitter content in the whole brain and spinal cord in VGAT(+/−) mice at 12 weeks old. Despite reduced expression of VGAT protein levels in VGAT(+/−) mice, there were no significant genotype differences in glutamate, GABA, and glycine levels (Table 1). Glycine levels in the spinal cord were approximately four times higher than GABA in both genotypes, whereas GABA levels were dominant in the brain. HPLC data include synaptic vesicular, intracellular, and extracellular (ambient) contents, indicating that the total amount of GABA and glycine are unchanged in the CNS.

Behavioral Analysis of VGAT(+/−) Mice. WT mice and VGAT(+/−) mice were tested in measurements of spontaneous activity in the home cage, RotaRod, elevated plus maze, and Morris water maze. None of these assays showed significant difference between genotypes (Fig. 2; Table 2), indicating that VGAT(+/−) mice have normal motor coordination, anxiety level, and memory performance. In the RotaRod assay, both WT mice (n = 5) and VGAT(+/−) mice (n = 5) could stay on the rotating bar for more than 180 s in three consecutive trials. In the elevated plus maze test, no significant differences were found between WT mice and VGAT(+/−) mice in any parameters recorded (Table 2). In the Morris water maze test, genotype had no effect on ability to improve performance as result of training, although VGAT(+/−) mice reached the platform even faster than WT mice during early trials (Fig. 2B).

Thermal Hyperalgesia in VGAT(+/−) Mice. In the hot-plate test, licking or jumping responses were considered to be the result of supraspinal sensory integration (Caggiula et al., 1995; Rubinstein et al., 1996). To test the sensory performance at the supraspinal level, we first measured the latency to responses from the hot-plate set at 53°C (Fig. 3A). The cut-off latency was set at 60 s. A significant reduction in the latency was observed in VGAT(+/−) mice (21.0 ± 0.9 s, n = 20) compared with WT mice (24.4 ± 1.1 s, n = 20, $P < 0.05$), suggesting that nociceptive perception via supraspinal sites is increased in VGAT(+/−) mice.

Transmitter spillover between synapses is often enhanced after blockade of transmitter transporters. Given the dominant role of glycine in the spinal cord, we sought to determine whether glycine uptake systems would play any role in acute thermal nociception. Glycine transporters have been cloned and are classified into two distinct gene families, glycine transporter 1 (GlyT1) and glycine transporter 2 (GlyT2). Cellular expression studies have revealed that GlyT1 is distributed widely throughout the CNS and that distribution correlates better with the localization of NMDA receptors than with the strychnine-sensitive glycine receptor (Borowsky et al., 1993), suggesting

TABLE 1
GABA, glycine, and glutamate levels in the whole brain and spinal cord from WT mice and VGAT(+/−) mice
Data represent means ± S.E.M. of five mice per group.

Region and Neurotransmitter	Neurotransmitter Levels	
	WT	VGAT(+/−)
	nmol/g	
Whole brain		
GABA	4052.1 ± 308.2	3899.3 ± 147.5
Glycine	1628.8 ± 139.8	1571.3 ± 65.3
Glutamate	7137.9 ± 202.9	7575.6 ± 156.1
Spinal cord		
GABA	1035.6 ± 57.0	1078.0 ± 91.7
Glycine	4294.5 ± 128.6	4176.3 ± 140.1
Glutamate	4214.0 ± 52.6	4056.4 ± 70.7

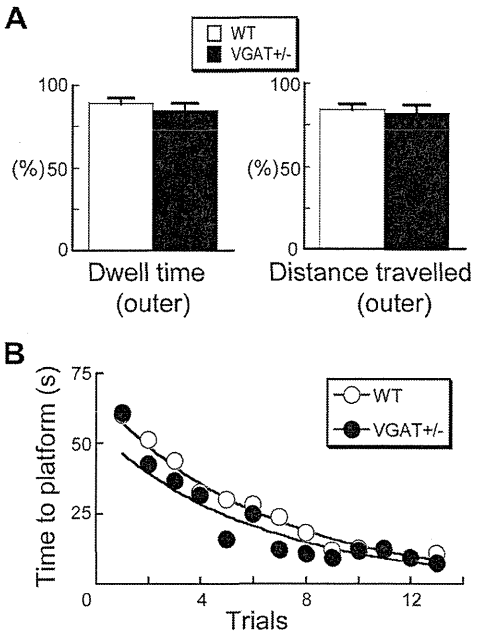

Fig. 2. A, VGAT(+/−) mice exhibit normal anxiety-like behaviors in the open field test. Regional dwell time in outer region (left) and regional distance traveled in outer region (right) was compared between genotypes (Student's t test, $n = 5$). B, performance of WT mice and VGAT(+/−) mice in the Morris water maze ($n = 10$ each). Learning curves for both genotypes show latencies to find the platform during trials.

that GlyT1 is involved in glycine supply for the activation of NMDA receptors. Intraperitoneal injection of *N*-[(3*R*)-3-([1,1'-biphenyl]-4-yloxy)-3-(4-fluorophenyl)propyl]-*N*-methylglycine hydrochloride (ALX-5407), a selective inhibitor of the GlyT1, dose dependently prolonged the latency in both WT mice ($n = 16$) and VGAT(+/−) mice ($n = 11$, Fig. 3A). Thus, ALX-5407 had an analgesic effect, perhaps by increasing tonic inhibition mediated by glycine receptors.

To test the sensory performance at the spinal cord level, responses to thermal nociception were examined using the tail-immersion test, which reflects spinally mediated reactions (Caggiula et al., 1995). We measured tail withdrawal latencies after tail immersion at 48 ± 0.5°C, and results are shown in Fig. 3B. There was no significant difference in the latency of the tail-immersion test ($n = 14$ each).

Enhanced Inflammatory Pain in VGAT(+/−) Mice. We examined whether the reduction of VGAT protein affected the behavioral responses of mice in an inflammatory pain model. Inflammatory pain involves an activity-dependent facilitation in excitability of both peripheral neurons (peripheral sensitization), and spinal and supraspinal neurons (central sensitization), including thalamus and cortex. To examine the contribution of VGAT to inflammatory pain signaling, we used the formalin test. The subcutaneous injection of formalin (5% formalin, 20 μl) produced a well known biphasic pattern of nociceptive behaviors in both genotypes (Fig. 4A). The nociceptive responses were mainly observed within 10 min of and 10 to 60 min after injection, which correspond to the early (phase 1) and late (phase 2) phases. Total time of lifting, licking, or flinching in phase 1 represents a response to chemical nociception as a result of tissue damage, whereas the responses in phase 2 are a response to subsequent inflammation. A behaviorally quiescent interphase, in which the animals showed very little nociceptive responses, was observed between two phases. Although no genotype difference was observed in total time of phase 1 responses ($n = 12$ each), phase 2 responses were significantly enhanced in VGAT(+/−) mice ($P < 0.05$ versus WT mice). We conclude that partial reduction of VGAT protein levels are involved in formalin-induced inflammatory pain signaling.

Behavioral Responses to Intravenous General Anesthetics Propofol and Ketamine Are Unchanged in VGAT(+/−) Mice. We then compared anesthetic sensitivity to an intravenous anesthetic propofol, a positive allosteric modulator of $GABA_A$ receptors. The latency to LORR produced by propofol (100 mg/kg i.p.) was similar between both genotypes ($n = 20$ each; Fig. 5A, left). The latency to LORR produced by ketamine (75 mg/kg i.p.), a NMDA receptor open-channel blocker, was also similar between both genotypes ($n = 12$ each; Fig. 5A, right). In addition, there was no significant difference in the duration of LORR produced by propofol (100 mg/kg i.p.) and ketamine (75 mg/kg i.p.) between genotypes (Fig. 5B). These data suggest that VGAT(+/−) mice have normal sensitivity to anesthetic drugs that produce hypnosis by enhancing GABAergic inhibition or by inhibiting NMDA receptors.

Glycinergic, but Not GABAergic, mIPSCs In the Spinal Cord Is Diminished in VGAT(+/−) Mice. Given behavioral effects of reduction of VGAT protein on acute nociception and inflammatory pain in VGAT(+/−) mice, we next tried to provide physiological evidence for the role of VGAT in inhibitory synaptic transmission. We tried to identify a functional correlation of reduction of VGAT protein for the phenotype observed in VGAT(+/−) mice. To study inhibitory synaptic transmission, we then looked at the influence of reduction of VGAT protein on spontaneous GABAergic and glycinergic synaptic currents in lamina II in the spinal cord. Action potential-independent components of $GABA_A$ receptor-mediated IPSCs [miniature IPSCs (mIPSCs)] and glycine receptor-mediated mIPSCs were recorded at 0 mV using Cs_2SO_4-based internal solutions in the presence of the sodium channel blocker tetrodotoxin (TTX; 1 μM). Under these conditions, mIPSCs were recorded as outward currents and excitatory postsynaptic currents were not detectable because the holding potential of 0 mV is near the reversal potential for excitatory postsynaptic currents.

Figure 6A shows representative traces of GABAergic (left) and glycinergic (right) mIPSCs from lamina II neurons in both genotypes. Bicuculline (10 μM) or strychnine (300 nM) was used to isolate glycinergic and GABAergic mIPSCs, respectively. Kinetic analysis revealed that the decay phase of GABAergic mIPSCs (19.9 ± 2.9 ms, $n = 6$) was significantly slower than that of strychnine-sensitive glycinergic mIPSCs (7.7 ± 1.1 ms, $n = 6$; $P < 0.01$). As reported earlier (Jonas et al., 1998; Keller et al., 2001), both GABAergic and glycinergic

TABLE 2
Elevated plus-maze performance of WT mice and VGAT(+/−)
Data represent mean ± S.E.M. of five mice. The mouse was placed in the center of the maze facing one of the enclosed arms and observed for 5 min.

Parameter	WT	VGAT(+/−)
Open arm duration, s	30.3 ± 3.2	35.8 ± 4.8
Closed arm duration, s	238.7 ± 13.8	230.9 ± 14.6
Central platform duration, s	30.6 ± 4.4	33.0 ± 3.4
Open arm frequency	6.3 ± 1.8	7.2 ± 1.4
Closed arm frequency	4.5 ± 1.2	6.5 ± 1.8

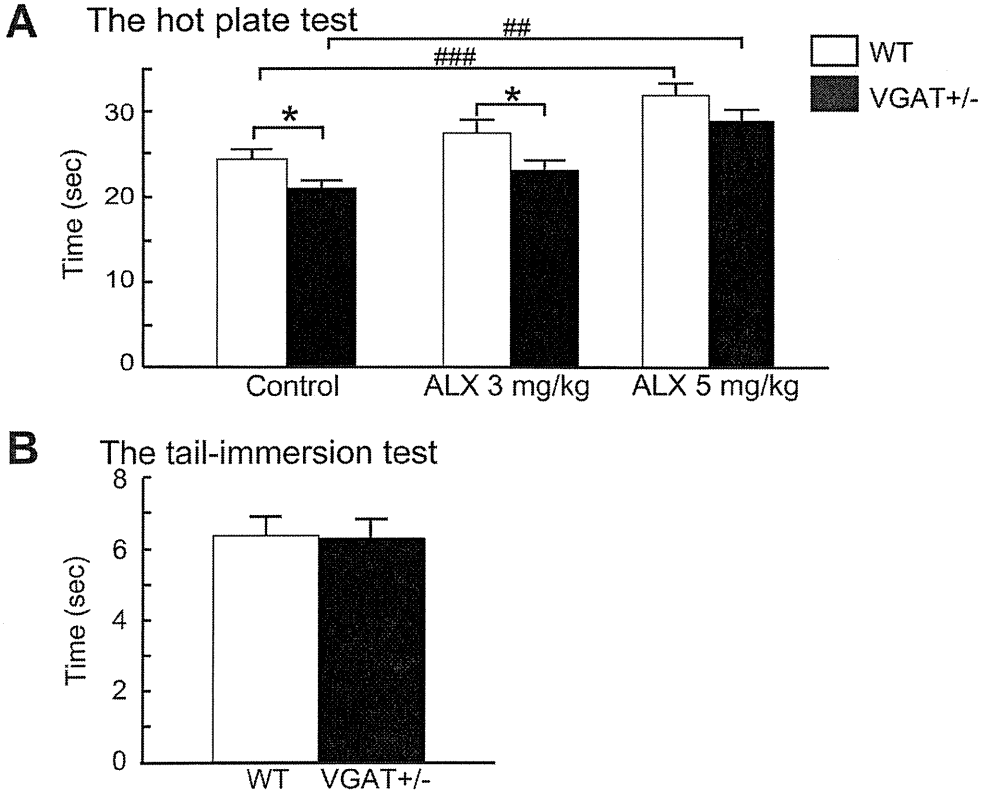

Fig. 3. Antinociceptive responses of WT mice and VGAT(+/−) mice in the hotplate test (53°C). A, the hotplate test revealed that the latency was significantly reduced in VGAT(+/−) mice (n = 20) compared with WT mice (n = 20; *, $P < 0.05$, Student's t test). ALX-5407, GlyT1 inhibitor, was injected intraperitoneally 24 h before the hotplate test. ALX-5407 dose dependently increased the latency in both genotypes. *, $P < 0.05$, comparison between genotypes (Student's t test); ##, $P < 0.01$ versus control in VGAT(+/−) mice; ###, $P < 0.001$ versus control in WT mice (one-way analysis of variance followed by the post hoc Tukey method). B, antinociceptive responses of WT mice and VGAT(+/−) mice in the tail-immersion test (48°C). The tail-immersion test, in which the response is considered to be a spinal reflex, is normal in VGAT(+/−) mice (Student's t test).

mIPSCs were observed in neurons of young mice (14–21 days old). These mixed GABAergic/glycinergic mIPSCs are the result from corelease of GABA and glycine at the same inhibitory synapse in spinal laminas I and II. The amplitude of GABAergic and glycinergic mIPSCs either displayed as the mean amplitude or as a cumulative probability distribution was significantly reduced in VGAT(+/−) mice ($P < 0.001$; Fig. 6B). Although the frequency of GABAergic mIPSCs was similar between genotypes, the frequency of glycinergic mIPSCs was significantly reduced in VGAT(+/−) mice (n = 7, $P < 0.01$ versus WT mice, n = 6, Fig. 6C), indicating that reduction of VGAT proteins affected the probability of glycine release.

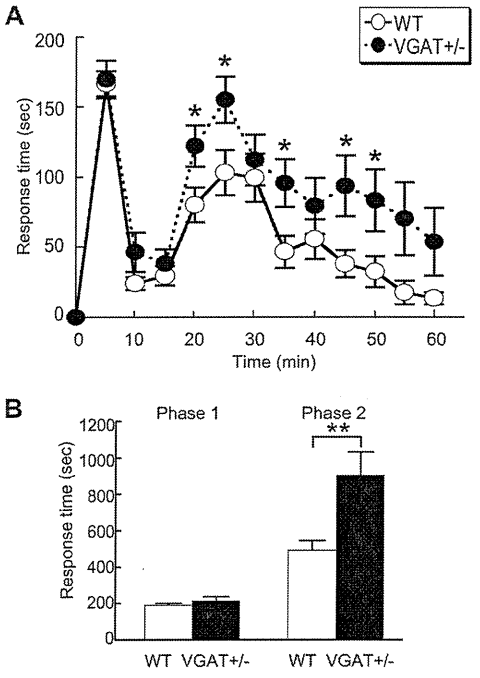

Fig. 4. The effects of partial reduction of VGAT on formalin-induced persistent pain. A, the time courses of the formalin-induced nociceptive responses in WT mice (○) and VGAT(+/−) mice (●) (n = 12, each). Total time of nociceptive response (seconds) per 5 min was measured. *, $P < 0.05$ between genotypes, Student's t test. B, the formalin-induced nociceptive responses of the initial 10-min period (phase 1) and the last 50-min period (phase 2) were compared between genotypes (**, $P < 0.01$).

Glycinergic, but Not GABAergic, Synaptic Transmission Stimulated by High Potassium Solutions Is Also Impaired in VGAT(+/−) Mice. We next compared the high potassium-induced potentiation of spontaneous glycine release in ACSF solutions including 2 mM Ca^{2+} in lamina II neurons using the whole-cell patch-clamp technique. Recordings were performed in the presence of bicuculline (10 μM), 6-cyano-2,3-dihydroxy-7-nitroquinoxaline (20 μM), D,L-2-amino-5-phosphonovalerate (100 μM), and TTX (1 μM), so that spontaneous responses observed in this condition were glycinergic mIPSCs. Bath application of high potassium (50 mM) evoked transient outward currents by direct depolarization of terminals and a secondary steady-state component in WT mice (Fig. 7A). These are thought to represent the massive release of glycine from the readily releasable pool (RRP) and the reserve pool, respectively (Mozhayeva et al., 2002; Moulder and Mennerick, 2005). On the other hand, hyperkalemic solution (50 mM) application failed to evoke an initial rapid peak response in VGAT(+/−) mice, although a secondary steady-state response was observed (Fig. 7A). As a result, the peak amplitude of evoked responses was significantly reduced in VGAT(+/−) mice compared with WT mice

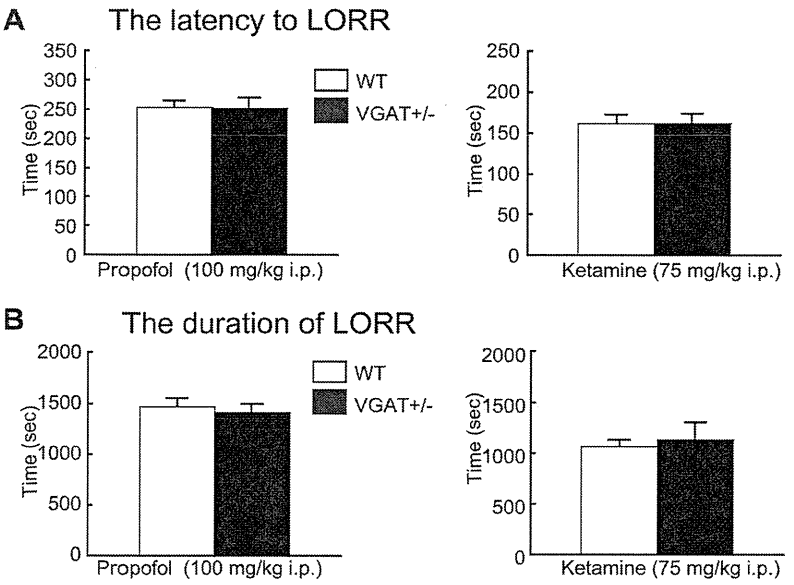

Fig. 5. Behavioral sensitivities to general anesthetics. A, the latency to LORR recorded from the time of propofol (100 mg/kg) or ketamine (75 mg/kg) injection. B, the duration of LORR produced by propofol (100 mg/kg) or ketamine (75 mg/kg).

($P < 0.05$, Fig. 7B), and the charge was also significantly reduced in VGAT(+/−) mice (Fig. 7C).

Discussion

Using mice with reduced expression of VGAT, we found that VGAT(+/−) mice showed enhanced sensitivity to thermal stimulation and chemical inflammation in an animal model. However, motor coordination, anxiety, memory performance, and behavioral responses to the anesthetics of VGAT(+/−) mice were unchanged. Glycinergic mIPSCs in the lamina II neurons during sustained stimulation by high potassium levels were diminished in VGAT(+/−) mice. On the basis of this evidence, we conclude that partial reduction of VGAT-mediated inhibitory drive alters very specific forms of sensory processing.

VGAT Protein Levels, Neurotransmitter Content, and Behavior. The *VGAT* gene is remarkably compact, spanning ~5 kilobase pairs in mice (Ebihara et al., 2003), and is expressed mainly in the CNS, where it localizes to the synaptic vesicles of GABAergic and glycinergic neurons (McIntire et al., 1997). It is also expressed in some peripheral tissues, including the pituitary and pineal glands and the pancreas (Gasnier, 2004). Thus, reduction of VGAT protein may affect not only behavioral performance but also higher brain function. In our tests, however, motor performance and spatial memory function were normal in VGAT(+/−) mice. In concurrence with previous observations (Saito et al., 2010), VGAT protein levels were reduced in VGAT(+/−) mice. HPLC assays revealed that, in both genotypes, glycine levels were dominant in the spinal cord, whereas GABA levels were dominant in the brain. These data are consistent with previous findings that glycine levels are highest in the spinal cord, pons, and medulla oblongata, regions in which glycine receptors (GlyRs) are predominantly expressed (Legendre, 2001).

The pain threshold resulting from glycinergic neuromechanisms is not always constant, because glycine content can be drastically up-regulated or down-regulated by various factors. For example, presynaptic membrane glycine transporters also play an important role in the control of neuronal excitability by modulating tonic glycinergic inhibition. We found that ALX-5407, a selective inhibitor of the glycine transporter GlyT1, prolonged the hotplate latency in both genotypes, suggesting that the sensitivity of mice to acute thermal pain is influenced by variation in GlyT1 function. However, because HPLC analysis cannot distinguish between synaptic vesicular, intracellular, and extracellular (ambient) content of glycine, the exact role of tonic glycinergic inhibition on the pain threshold should be further studied using a microdialysis assay.

The Distinct Role of GABA and Glycine in Sensory Processing. We reported previously that *GAD65* gene knockout and the resulting reduction in GABAergic inhibition altered anesthetic sensitivity to propofol and short-term thermal nociception without affecting the inflammatory pain threshold (Kubo et al., 2009a; Kubo et al., 2009b). In contrast, in the present study, we found that VGAT-mediated reduction of glycinergic inhibition enhanced short-term thermal nociception and inflammatory pain without affecting behavioral sensitivity to propofol and ketamine. In the formalin test, genotype differences were evident only in phase II, which was enhanced in VGAT(+/−) mice, although reduction of VGAT protein did not affect responses in phase I. Phase I responses are evoked by direct chemical activation of peripheral C-fibers, whereas phase II responses depend on local inflammation and/or subsequent sensitization of nociceptive neurons (Rosland et al., 1990). These data support the hypothesis that GABA and glycine may have distinct roles in pain signal transduction. As an example to support this notion, strychnine, a selective competitive antagonist of glycine at the postsynaptic membrane, induces morphine-resistant dynamic, but not static, mechanical allodynia in rats, whereas bicuculline, a competitive antagonist of the $GABA_A$ receptor, induces static, but not dynamic, allodynia (Miraucourt et al., 2009). In addition, Inquimbert et al. (2007) compared the properties of inhibitory synaptic transmission in laminae II, III, and IV of the dorsal horn, which are involved in the processing of nociceptive and non-nociceptive sensory information. Fifty-five percent of lamina II neurons received both GABAergic and glycinergic inputs, suggesting that lam-

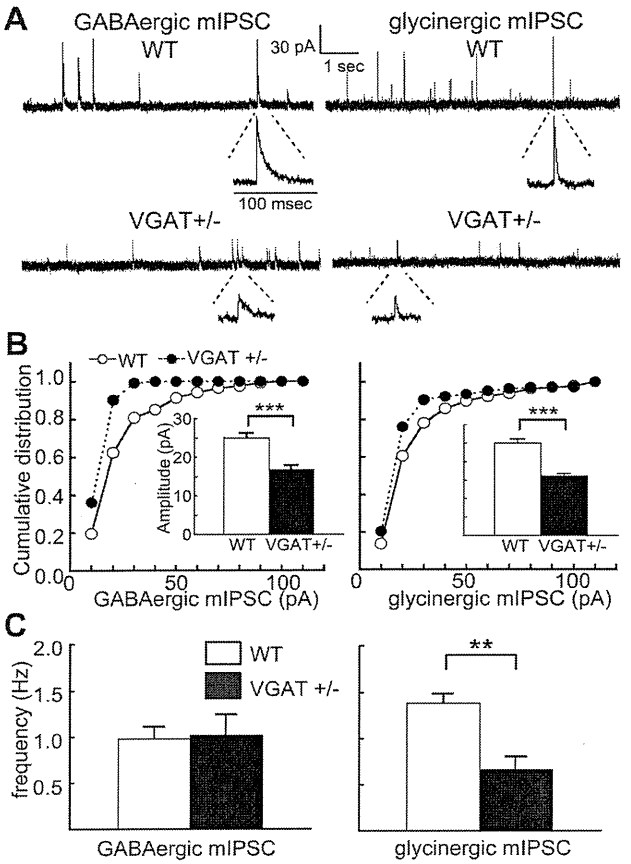

Fig. 6. Isolation of GABAergic and glycinergic mIPSCs in lamina II neurons of young WT mice and VGAT(+/−) mice. A, sample traces show GABAergic mIPSCs (left) and glycinergic mIPSCs (right) from WT mice (top) and VGAT(+/−) mice (bottom). Neurons were voltage-clamped at 0 mV using Cs_2SO_4-based internal solutions. Enlarged mIPSCs are also shown to compare the decay phase. B, cumulative distribution and mean amplitude of mIPSCs were compared between genotypes. ***, $P < 0.001$ versus corresponding WT mice (Student's t test). C, the frequency of mIPSCs was compared between genotypes. **, $P < 0.01$ versus corresponding WT mice (Student's t test).

ina II neurons, which play a crucial role in nociceptive processing, are regulated by glycinergic inhibition.

The Role of Glycine and Glycine Receptors in Inflammatory Pain. The amplitude of GABAergic and glycinergic mIPSCs was significantly reduced in lamina II neurons of VGAT(+/−) mice, suggesting that reduced VGAT protein levels led to a reduced content of GABA and glycine in the vesicles. The total GABA and glycine content per vesicle may therefore be sensitive to VGAT protein levels. In addition, significant genotype differences in glycine release were observed in the presence of solutions containing high levels of potassium. These results suggest that, during sustained stimulation, the increase in glycine release is probably not maintained in VGAT(+/−) mice. The loading of transmitters, mobilization of vesicles, and/or replenishment of vesicles at release sites that normally occur in WT mice during sustained stimulation, such as with inflammatory pain, may be impaired in VGAT(+/−) mice. A frequently used technique to evaluate the size of the RRP is hypertonic sucrose application (0.5 mM) in autaptic synapses in cell culture. We also tried to apply hypertonic sucrose solution (0.5 mM, $n = 3$) instead of high-potassium solutions to deplete the RRP. Unfortunately, we could not complete these experiments in slice preparations because the tight seal was broken after sucrose application, presumably as a result of changes in the osmotic pressure of neurons.

Tonic inhibition is a key regulator of inhibitory tone in several brain regions (Farrant and Nusser, 2005) and in the dorsal horn (Mitchell et al., 2007). GlyRs are pentameric ion channels composed of α1-α4 and β subunits (Legendre, 2001; Lynch, 2004). RNA edited α2- and α3-GlyRs may serve a particular function as extrasynaptic high-affinity GlyRs in the hippocampus (Meier et al., 2005); little is known about the role of tonic inhibition mediated by GlyRs in the dorsal horn. GlyRα3 is an adult glycine receptor subunit that is much less abundant than GlyRα1 but plays an important role in inflammatory pain sensation, because GlyRα3 is predominantly expressed in superficial layers of the spinal cord dorsal horn, where nociceptive afferents terminate. The central component of sensitization to inflammatory pain is disinhibition of dorsal horn neurons, which are relieved from glycinergic inhibition by the inflammatory mediator prostaglandin E2 (PGE2) (Ahmadi et al., 2002). PGE2 activates

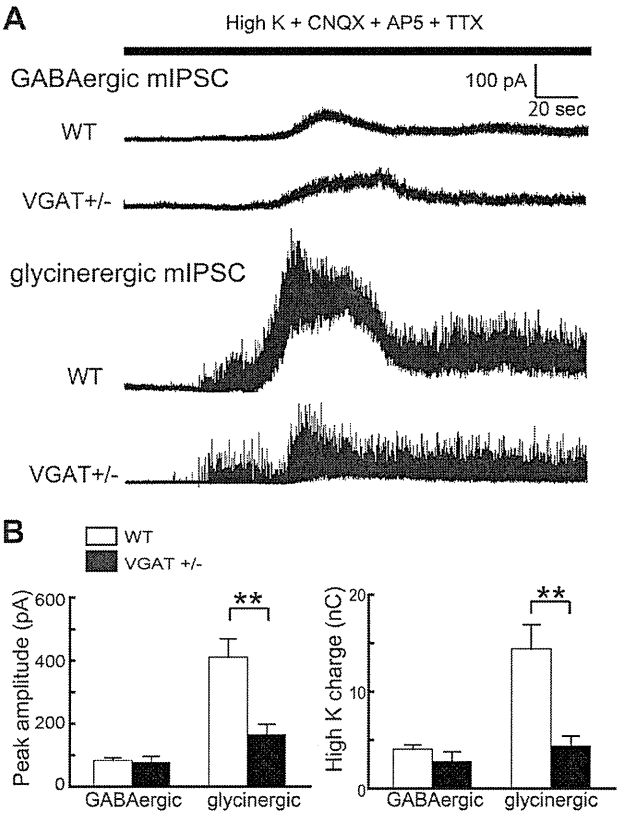

Fig. 7. The high potassium-induced potentiation of glycinergic, but not GABAergic, mIPSCs in lamina II neurons of young WT mice and VGAT(+/−) mice. A, representative traces of isolated GABAergic and glycinergic mIPSCs of WT mice and VGAT(+/−) mice. Currents were recorded in the presence of 6-cyano-2,3-dihydroxy-7-nitroquinoxaline (CNQX), D,L-2-amino-5-phosphonovalerate (AP5), TTX, and strychnine (for GABAergic mIPSC) or bicuculline (for glycinergic mIPSC). B, peak amplitudes of potassium-evoked currents were compared between genotypes [GABAergic, WT, $n = 8$, VGAT(+/−), $n = 6$; glycinergic, WT, $n = 6$, VGAT(+/−), $n = 9$]. **, $P < 0.01$ versus corresponding WT mice (Student's t test). C, charges of potassium-evoked currents were compared between genotypes [GABAergic: WT, $n = 8$, VGAT(+/−), $n = 6$; glycinergic, WT, $n = 6$, VGAT(+/−), $n = 9$]. **, $P < 0.01$ versus corresponding WT mice (Student's t test).

prostaglandin E receptors of the EP2 subtype and leads to protein kinase A-dependent phosphorylation and inhibition of synaptic GlyRs containing the α3 subunit (Harvey et al., 2004). Mice deficient in GlyR α3 not only lack the inhibition of glycinergic neurotransmission by PGE2 seen in WT mice but also show a reduction in pain sensitization induced by spinal PGE2 injection or peripheral inflammation. These results suggest that therapies aimed at glycinergic inhibition mediated by α3 subunits of GlyR may prove effective in the management of chronic inflammatory pain.

Study Limitations. Although we tried to elucidate the relative contributions of VGAT on in vivo pain and anesthetic sensitivity, this study has some limitations. First, mice in different developmental stages were used in this study. Although adult mice 12 to 16 weeks of age were used for behavioral assays, young mice (postnatal days 14–21) were used for electrophysiological analysis, because neurons in slice preparations could be visually identified by their relative translucency as a result of the lack of myelination in young mice (Yoshimura and Nishi, 1993). However, chloride homeostasis and the relative expression of GABA and glycine receptors in lamina II neurons may be changing during this stage (Jonas et al., 1998; Keller et al., 2001). These two studies used rats, not mice; this prevents direct comparison in terms of developmental stage of GABAergic and glycinergic neurotransmission. Therefore, our data lack convincing evidence that altered glycinergic transmission in young mice is directly linked with the behavioral observations in adult mice. Second, Western blot analysis showed that VGAT protein of VGAT(+/−) mice was reduced compared with WT mice, but there is no evidence for a change in GABA or glycine levels. In this context, it seems critical to establish that GABA/glycine uptake into synaptic vesicles is actually affected by reduced VGAT expression. However, it is technically difficult to quantify GABA/glycine uptake in a synaptosome-enriched fraction of the spinal cord (Hell and Jahn 1998). Finally, recent evidence shows that neurons in the CNS seem to contain an as-yet unknown vesicular transport system for GABA and glycine with VGAT-like substrate specificity, because some VGAT-deficient neurons still show measurable vesicular release of the two transmitters (Wojcik et al., 2006). Further examination will be needed to confirm the role of VGAT to behavioral responses in vivo.

Possible Indications of VGAT as a Therapeutic Target. GABA receptors contribute successful drug targets in the treatment of anxiety, sleep disorders, epilepsy, and general anesthesia, whereas drugs specifically targeting glycine are currently lacking. Previous studies have revealed that an increase in the extracellular concentrations of glycine in the spinal cord by blocking its uptake via membrane glycine transporters generates analgesic effects on neuropathic pain (Morita et al., 2008; Tanabe et al., 2008). The present study provides new evidence that VGAT, which belongs to a eukaryotic-specific superfamily of H^+-coupled amino acid transporters and regulates the uptake of neurotransmitter sequestered in synaptic vesicles (McIntire et al., 1997; Sagné et al., 1997), may be a therapeutic drug target for the treatment of inflammatory pain.

Acknowledgments

We thank Masae Iino, Toshikazu Kakizaki, and Ying Wang for technical assistance in patch-clamp recordings or Western blot analysis, Shigeo Takamori for providing antibodies against VGAT, and M. Bruce MacIver and Yasuhiko Saito for critical comments on the manuscript. We also thank the staff at Institute of Experimental Animal Research, Gunma University Graduate School of Medicine, for assistance in animal care.

Authorship Contributions

Participated in research design: Yamada, Nishikawa, Kubo, Yanagawa, and Saito.

Conducted experiments: Yamada, Nishikawa, and Kubo.

Performed data analysis: Yamada and Nishikawa.

Contributed to the writing of the manuscript: Yamada and Nishikawa.

References

Ahmadi S, Lippross S, Neuhuber WL, and Zeilhofer HU (2002) PGE(2) selectively blocks inhibitory glycinergic neurotransmission onto rat superficial dorsal horn neurons. *Nat Neurosci* **5:**34–40.

Betz H and Laube B (2006) Glycine receptors: recent insights into their structural organization and functional diversity. *J Neurochem* **97:**1600–1610.

Borowsky B, Mezey E, and Hoffman BJ (1993) Two glycine transporter variants with distinct localization in the CNS and peripheral tissues are encoded by a common gene. *Neuron* **10:**851–863.

Caggiula AR, Epstein LH, Perkins KA, and Saylor S (1995) Different methods of assessing nicotine-induced antinociception may engage different neural mechanisms. *Psychopharmacology* **122:**301–306.

Chaudhry FA, Reimer RJ, Bellocchio EE, Danbolt NC, Osen KK, Edwards RH, and Storm-Mathisen J (1998) The vesicular GABA transporter, VGAT, localizes to synaptic vesicles in sets of glycinergic as well as GABAergic neurons. *J Neurosci* **18:**9733–9750.

Dubuisson D and Dennis SG (1977) The formalin test: a quantitative study of the analgesic effects of morphine, meperidine, and brain stem stimulation in rats and cats. *Pain* **4:**161–174.

Dumoulin A, Rostaing P, Bedet C, Lévi S, Isambert MF, Henry JP, Triller A, and Gasnier B (1999) Presence of the vesicular inhibitory amino acid transporter in GABAergic and glycinergic synaptic terminal boutons. *J Cell Sci* **112:**811–823.

Ebihara S, Obata K, and Yanagawa Y (2003) Mouse vesicular GABA transporter gene: genomic organization, transcriptional regulation and chromosomal localization. *Brain Res Mol Brain Res* **110:**126–139.

Farrant M and Nusser Z (2005) Variations on an inhibitory theme: phasic and tonic activation of GABA(A) receptors. *Nat Rev Neurosci* **6:**215–229.

Furue H, Katafuchi T, and Yoshimura M (2004) Sensory processing and functional reorganization of sensory transmission under pathological conditions in the spinal dorsal horn. *Neurosci Res* **48:**361–368.

Gasnier B (2004) The SLC32 transporter, a key protein for the synaptic release of inhibitory amino acids. *Pflugers Arch* **447:**756–759.

Harvey RJ, Depner UB, Wässle H, Ahmadi S, Heindl C, Reinold H, Smart TG, Harvey K, Schütz B, Abo-Salem OM, et al. (2004) GlyR alpha3: an essential target for spinal PGE2-mediated inflammatory pain sensitization. *Science* **304:**884–887.

Hell JW and Jahn R (1998) Bioenergetic characterization of gamma-aminobutyric acid transporter of synaptic vesicles. *Methods Enzymol* **296:**116–124.

Inquimbert P, Rodeau JL, and Schlichter R (2007) Differential contribution of GABAergic and glycinergic components to inhibitory synaptic transmission in lamina II and laminae III-IV of the young rat spinal cord. *Eur J Neurosci* **26:**2940–2949.

Jonas P, Bischofberger J, and Sandkühler J (1998) Corelease of two fast neurotransmitters at a central synapse. *Science* **281:**419–424.

Keller AF, Coull JA, Chery N, Poisbeau P, and De Koninck Y (2001) Region-specific developmental specialization of GABA-glycine cosynapses in laminas I-II of the rat spinal dorsal horn. *J Neurosci* **21:**7871–7880.

Kubo K, Nishikawa K, Hardy-Yamada M, Ishizeki J, Yanagawa Y, and Saito S (2009a) Altered responses to propofol, but not ketamine, in mice deficient in the 65-kilodalton isoform of glutamate decarboxylase. *J Pharmacol Exp Ther* **329:**592–599.

Kubo K, Nishikawa K, Ishizeki J, Hardy-Yamada M, Yanagawa Y, and Saito S (2009b) Thermal hyperalgesia via supraspinal mechanisms in mice lacking glutamate decarboxylase 65. *J Pharmacol Exp Ther* **331:**162–169.

Legendre P (2001) The glycinergic inhibitory synapse. *Cell Mol Life Sci* **58:**760–793.

Lynch JW (2004) Molecular structure and function of the glycine receptor chloride channel. *Physiol Rev* **84:**1051–1095.

Masson J, Sagné C, Hamon M, and El Mestikawy S (1999) Neurotransmitter transporters in the central nervous system. *Pharmacol Rev* **51:**439–464.

McIntire SL, Reimer RJ, Schuske K, Edwards RH, and Jorgensen EM (1997) Identification and characterization of the vesicular GABA transporter. *Nature* **389:**870–876.

Meier JC, Henneberger C, Melnick I, Racca C, Harvey RJ, Heinemann U, Schmieden V, and Grantyn R (2005) RNA editing produces glycine receptor alpha3(P185L), resulting in high agonist potency. *Nat Neurosci* **8:**736–744.

Mihic SJ, Ye Q, Wick MJ, Koltchine VV, Krasowski MD, Finn SE, Mascia MP, Valenzuela CF, Hanson KK, Greenblatt EP, et al. (1997) Sites of alcohol and volatile anaesthetic action on GABA(A) and glycine receptors. *Nature* **389:**385–389.

Miraucourt LS, Moisset X, Dallel R, and Voisin DL (2009) Glycine inhibitory dysfunction induces a selectively dynamic, morphine-resistant, and neurokinin 1 receptor- independent mechanical allodynia. *J Neurosci* **29:**2519–2527.

Mitchell EA, Gentet LJ, Dempster J, and Belelli D (2007) GABAA and glycine receptor-mediated transmission in rat lamina II neurones: relevance to the analgesic actions of neuroactive steroids. *J Physiol* **583:**1021–1040.
Morita K, Motoyama N, Kitayama T, Morioka N, Kifune K, and Dohi T (2008) Spinal antiallodynia action of glycine transporter inhibitors in neuropathic pain models in mice. *J Pharmacol Exp Ther* **326:**633–645.
Moulder KL and Mennerick S (2005) Reluctant vesicles contribute to the total readily releasable pool in glutamatergic hippocampal neurons. *J Neurosci* **25:** 3842–3850.
Mozhayeva MG, Sara Y, Liu X, and Kavalali ET (2002) Development of vesicle pools during maturation of hippocampal synapses. *J Neurosci* **22:**654–665.
Nishikawa K, Jenkins A, Paraskevakis I, and Harrison NL (2002) Volatile anesthetic actions on the GABAA receptors: contrasting effects of alpha 1(S270) and beta 2(N265) point mutations. *Neuropharmacology* **42:**337–345.
Nishikawa K, Kubo K, Obata H, Yanagawa Y, and Saito S (2011) The influence of manipulations to alter ambient GABA concentrations on the hypnotic and immobilizing actions produced by sevoflurane, propofol, and midazolam. *Neuropharmacology* **61:**172–180.
Nishikawa K and MacIver MB (2000) Membrane and synaptic actions of halothane on rat hippocampal pyramidal neurons and inhibitory interneurons. *J Neurosci* **20:**5915–5923.
Price TJ, Cervero F, Gold MS, Hammond DL, and Prescott SA (2009) Chloride regulation in the pain pathway. *Brain Res Rev* **60:**149–170.
Rosland JH, Tjølsen A, Maehle B, and Hole K (1990) The formalin test in mice: effect of formalin concentration. *Pain* **42:**235–242.
Rubinstein M, Mogil JS, Japón M, Chan EC, Allen RG, and Low MJ (1996) Absence of opioid stress-induced analgesia in mice lacking beta-endorphin by site-directed mutagenesis. *Proc Natl Acad Sci USA* **93:**3995–4000.
Sagné C, El Mestikawy S, Isambert MF, Hamon M, Henry JP, Giros B, and Gasnier B (1997) Cloning of a functional vesicular GABA and glycine transporter by screening of genome databases. *FEBS Lett* **417:**177–183.
Saito K, Kakizaki T, Hayashi R, Nishimaru H, Furukawa T, Nakazato Y, Takamori S, Ebihara S, Uematsu M, Mishina M, et al. (2010) The physiological roles of vesicular GABA transporter during embryonic development: a study using knockout mice. *Mol Brain* **3:**40.
Schenk F and Morris RG (1985) Dissociation between components of spatial memory in rats after recovery from the effects of retrohippocampal lesions. *Exp Brain Res* **58:**11–28.
Takamori S, Riedel D, and Jahn R (2000) Immunoisolation of GABA-specific synaptic vesicles defines a functionally distinct subset of synaptic vesicles. *J Neurosci* **20:**4904–4911.
Tanabe M, Takasu K, Yamaguchi S, Kodama D, and Ono H (2008) Glycine transporter inhibitors as a potential therapeutic strategy for chronic pain with memory impairment. *Anesthesiology* **108:**929–937.
Wojcik SM, Katsurabayashi S, Guillemin I, Friauf E, Rosenmund C, Brose N, and Rhee JS (2006) A shared vesicular carrier allows synaptic corelease of GABA and glycine. *Neuron* **50:**575–587.
Yoshimura M and Nishi S (1993) Blind patch-clamp recordings from substantia gelatinosa neurons in adult rat spinal cord slices: pharmacological properties of synaptic currents. *Neuroscience* **53:**519–526.
Zeilhofer HU (2005) The glycinergic control of spinal pain processing. *Cell Mol Life Sci* **62:**2027–2035.

Address correspondence to: Koichi Nishikawa, Department of Anesthesiology, Wakayama Medical University, 811-1 Kimiidera, Wakayama City 641-0012, Japan. E-mail: gaba-gly@wakayama-med.ac.jp

Maturation of Spinal Motor Neurons Derived from Human Embryonic Stem Cells

Tomonori Takazawa[1,7], Gist F. Croft[2,3,4,5,6,7], Mackenzie W. Amoroso[2,3,4,5,7], Lorenz Studer[8], Hynek Wichterle[2,3,4,5,6,7], Amy B. MacDermott[1,2,7]*

1 Department of Physiology and Cellular Biophysics, Columbia University, New York, New York, United States of America, **2** Department of Neuroscience, Columbia University, New York, New York, United States of America, **3** Department of Pathology, Columbia University, New York, New York, United States of America, **4** Department of Neurology, Columbia University, New York, New York, United States of America, **5** Center for Motor Neuron Biology and Disease, Columbia University, New York, New York, United States of America, **6** Columbia Stem Cell Initiative, Columbia University, New York, New York, United States of America, **7** Project A.L.S./Jenifer Estess Laboratory for Stem Cell Research, New York, New York, United States of America, **8** Centre for Stem Cell Biology, Sloan-Kettering Institute for Cancer Research, New York, New York, United States of America

Abstract

Our understanding of motor neuron biology in humans is derived mainly from investigation of human postmortem tissue and more indirectly from live animal models such as rodents. Thus generation of motor neurons from human embryonic stem cells and human induced pluripotent stem cells is an important new approach to model motor neuron function. To be useful models of human motor neuron function, cells generated *in vitro* should develop mature properties that are the hallmarks of motor neurons *in vivo* such as elaborated neuronal processes and mature electrophysiological characteristics. Here we have investigated changes in morphological and electrophysiological properties associated with maturation of neurons differentiated from human embryonic stem cells expressing GFP driven by a motor neuron specific reporter (*Hb9*::GFP) in culture. We observed maturation in cellular morphology seen as more complex neurite outgrowth and increased soma area over time. Electrophysiological changes included decreasing input resistance and increasing action potential firing frequency over 13 days *in vitro*. Furthermore, these human embryonic stem cell derived motor neurons acquired two physiological characteristics that are thought to underpin motor neuron integrated function in motor circuits; spike frequency adaptation and rebound action potential firing. These findings show that human embryonic stem cell derived motor neurons develop functional characteristics typical of spinal motor neurons *in vivo* and suggest that they are a relevant and useful platform for studying motor neuron development and function and for modeling motor neuron diseases.

Citation: Takazawa T, Croft GF, Amoroso MW, Studer L, Wichterle H, et al. (2012) Maturation of Spinal Motor Neurons Derived from Human Embryonic Stem Cells. PLoS ONE 7(7): e40154. doi:10.1371/journal.pone.0040154

Editor: Shawn Hochman, Emory University, United States of America

Received February 24, 2012; **Accepted** June 1, 2012; **Published** July 3, 2012

Funding: This work was supported by: Project A.L.S./Jenifer Estess Laboratory for Stem Cell Research; P2 ALS; NYSTEM grant CO24415; The Dr. Leigh G. Cascarilla Post-Doctoral Fellowships in Stem Cell Research; National Institutes of Health 1RC2NS069395. The funders had no role in study design, data collection and analysis, decision to publish, or preparation of the manuscript.

Competing Interests: The authors have declared that no competing interests exist.

* E-mail: abm1@columbia.edu

Introduction

Motor neurons are the final connecting link between the central nervous system and skeletal muscles. They are typically large neurons with extensive dendritic fields, primarily located in the ventral horn of the spinal cord. In humans, these neurons are essentially inaccessible for study. Therefore, most of our understanding of motor neuron development and function is based on studies in a variety of mammalian model systems such as cats and rodents, extensively reviewed in [1]. Recent demonstration that human embryonic stem (hES) cells can be induced to become motor neurons (hESMNs) [2,3,4] has made it possible to have reliable and direct access to human motor neurons for studies of development, function and pathology.

There are several hallmarks of mammalian motor neuron maturation to which maturation of hESMN can be compared. Most noticeably, as motor neurons develop, their soma size increases and they grow morphologically more complex [5,6]. Membrane properties also change developmentally with a decrease in input resistance, increasingly hyperpolarized resting membrane potentials and appearance of a repetitive firing response to a sustained depolarizing stimulus [5,7,8,9].

Many motor neurons show additional characteristic membrane properties. For example, many motor neurons have spike frequency adaptation (SFA), defined as an increase in inter spike interval (ISI) during a repetitive firing response to a steady depolarizing current [10,11,12]. SFA patterns of firing during the first few seconds of repetitive action potential activity have been thought to contribute to optimal development of sustained muscle contraction and thus to smooth muscle movements [13]. There is also evidence that activity dependent modulation of SFA can occur, especially to SFA that develops over seconds [14], raising the possibility that SFA may contribute to motor neuron function in a dynamic way. Another physiological feature of some motor neurons is a post inhibitory rebound depolarization that can drive action potential firing called rebound action potentials (RAP) [15,16]. RAP is a bursting discharge pattern that may contribute

to rhythmic bursting and interact with central pattern generated rhythmic firing [17].

A variety of motor neuron-like characteristics have been demonstrated in stem cell-derived motor neurons. When mouse and human stem cells are differentiated into motor neurons [2,3,4], both express the motor neuron specific transcription factor HB9 and when these neurons are transplanted *in vivo*, both have the ability to extend axons in the host ventral root towards target muscles [2,18]. Furthermore, mouse ES cell-derived motor neurons show some characteristic maturation-associated changes in membrane properties of motor neurons such as hyperpolarization of resting membrane potential and decreased input resistance [12]. However, several motor neuron properties that may contribute to regulated spike firing behavior have not been studied including SFA and RAP. These two properties, while not unique to motor neurons and not observed in all motor neurons, are broadly expressed in motor neuron populations.

Here we have examined whether hESMNs maturing *in vitro* develop characteristic motor neuron properties consistent with function in motor neuronal circuits including SFA and RAP. To accomplish this, hESMNs differentiated from stem cells and expressing GFP driven by a motor neuron specific reporter (*Hb9*::GFP) [2,19] were subjected to morphological and electrophysiological analysis by whole-cell patch clamp. We found progressive maturation in morphological and electrophysiological properties of hESMNs with time *in vitro*.

Results

Morphological Maturation of hESMNs in Vitro

One measure of maturation of hESMNs *in vitro* was documented by quantifying cell morphometry. Motor neurons were differentiated according to previously published protocols [3,20] with minor modifications (Fig. 1A; see Materials and Methods). Because only a minority of differentiated cells were motor neurons, we utilized a motor neuron reporter hES cell line, where GFP expression was driven by the motor neuron specific promoter of the transcription factor HB9 [19]. GFP was useful for measurement of morphological features and allowed identification of motor neurons in cultures prior to electrophysiological recording. Embryoid bodies (EBs) began to express HB9 protein and *Hb9*::GFP at day 25 (data not shown). EBs were dissociated to single cells on day 31 then cryopreserved for subsequent thaw and use in morphological and electrophysiological studies. Days *in vitro* (DIV) are indicated as day 31 plus the number of days in culture after being thawed.

To confirm the fidelity of GFP reporter expression within the $HB9^+$ populations of neurons, cells from a day 31+5 coverslip were immunostained for both GFP and HB9 (Fig. 1B). Automated cell scoring accurately identified cells positive for either marker based on very high intensity staining (Fig. 1B). Using the criteria described in Materials and Methods, we found that 87.8% of GFP^+ cells ($n = 250$ cells) were $HB9^+$, similar to the 66% reported previously for this cell line [19]. Thus, the *Hb9*::GFP reporter could be used to identify hESMNs.

Morphological changes, including soma size, branching and neurite outgrowth, began shortly after hESMNs were plated. Changes in cellular morphology were monitored from day 31+0 to 31+9 *in vitro*. Camera lucida tracing of representative cells at 3 different days in culture are shown in Figure 1C. An increase in the extent and complexity of neurite outgrowth is apparent by comparing morphology at day 31+2, 31+5 and 31+9 (Fig. 1C). Cell body area, number of branches and total neurite outgrowth increased significantly during the observation period (Fig. 1D–F) as did the number of primary neurites or processes per cell (data not shown). These data establish a timeline for morphological maturation that can be correlated with physiological changes.

Changes in Passive and Active Membrane Properties

The electrophysiological maturation of hESMNs over time *in vitro* was investigated by recording passive and active membrane properties from GFP expressing neurons. To confirm that recordings were accurately made on GFP-expressing motor neurons, some of the cells were loaded with biocytin during recording. They were then fixed and stained for both biocytin and GFP. Double labeling (e.g. Fig. 2A–C, E, G, I), confirmed that the neurons under study were hESMNs.

Examples of membrane potential changes in response to depolarizing and hyperpolarizing current steps together with a biocytin, GFP, DAPI triple stained image of the recorded hESMNs are shown in Figure 2D–I for 3 different hESMNs at 31+5, 31+9 and 31+13 DIV. In these examples, membrane potential responses to injected currents are clearly different among the three cells, even though all three neurons fired action potentials with stronger depolarizing stimuli. Because some of the action potentials occurring later in the trains became poorly defined, we set a criterion for identification of action potentials. Specifically, an action potential was operationally defined as having a threshold or inflection point just prior to the rapidly rising phase and a peak that overshoots 0 mV.

One of the clear changes in membrane properties observed as the hESMNs matured in culture was a decrease in input resistance (Fig. 2D,F,H) revealed by smaller changes in membrane potential elicited by hyperpolarizing current injections. These membrane properties are compared quantitatively over time *in vitro* in Figure 3A. Input resistance decreased with increasing DIV (Fig. 3A, $n = 28$, $P<0.01$, one-way ANOVA), suggesting an increase in the total number of channels contributing to leak conductance at resting membrane potential. There was no significant change in resting membrane potential over the time frame of *in vitro* maturation tested here (Fig. 3B).

In all except one of the hESMNs tested ($n = 28/29$), at least one action potential could be evoked by depolarizing current. The one exception was a day 31+2 neuron that had been grown only 2 DIV after plating, the earliest of the days tested. Action potentials were evoked by injecting depolarizing current from resting membrane potential. Rheobase, the minimum current step required to evoke action potentials, did not change with days *in vitro* (Fig. 3C). This lack of change of rheobase in the face of decreasing input resistance predicts an accompanying hyperpolarizing change in voltage threshold. Figure 3D shows that voltage threshold changes significantly from -19 mV to -33 mV between 31+2 and 31+12/31+13 DIV ($n = 29$, $P<0.001$, one-way ANOVA). The mean duration of action potentials (i.e. half-width of action potentials) also decreased with DIV (Fig. 3E, $n = 25$, $P<0.01$, one-way ANOVA), a typical change that accompanies maturation.

Because motor neurons develop the ability to fire repetitively as they mature [9], we investigated whether a similar change occurred as the hESMNs matured in culture. None of the neurons at the youngest age tested (31+2 DIV) could produce more than a single action potential during 1 sec depolarizing current steps. However, hESMNs acquired the ability to fire a train of action potentials over time *in vitro* (Fig. 2D, 2F and 2H). Maximum frequency of action potential firing in response to depolarizing current pulses increased with DIV (Fig. 3F, $n = 28$, $P<0.05$, one-way ANOVA), although the individual values in the same age groups showed considerable variation. Some neurons at the oldest

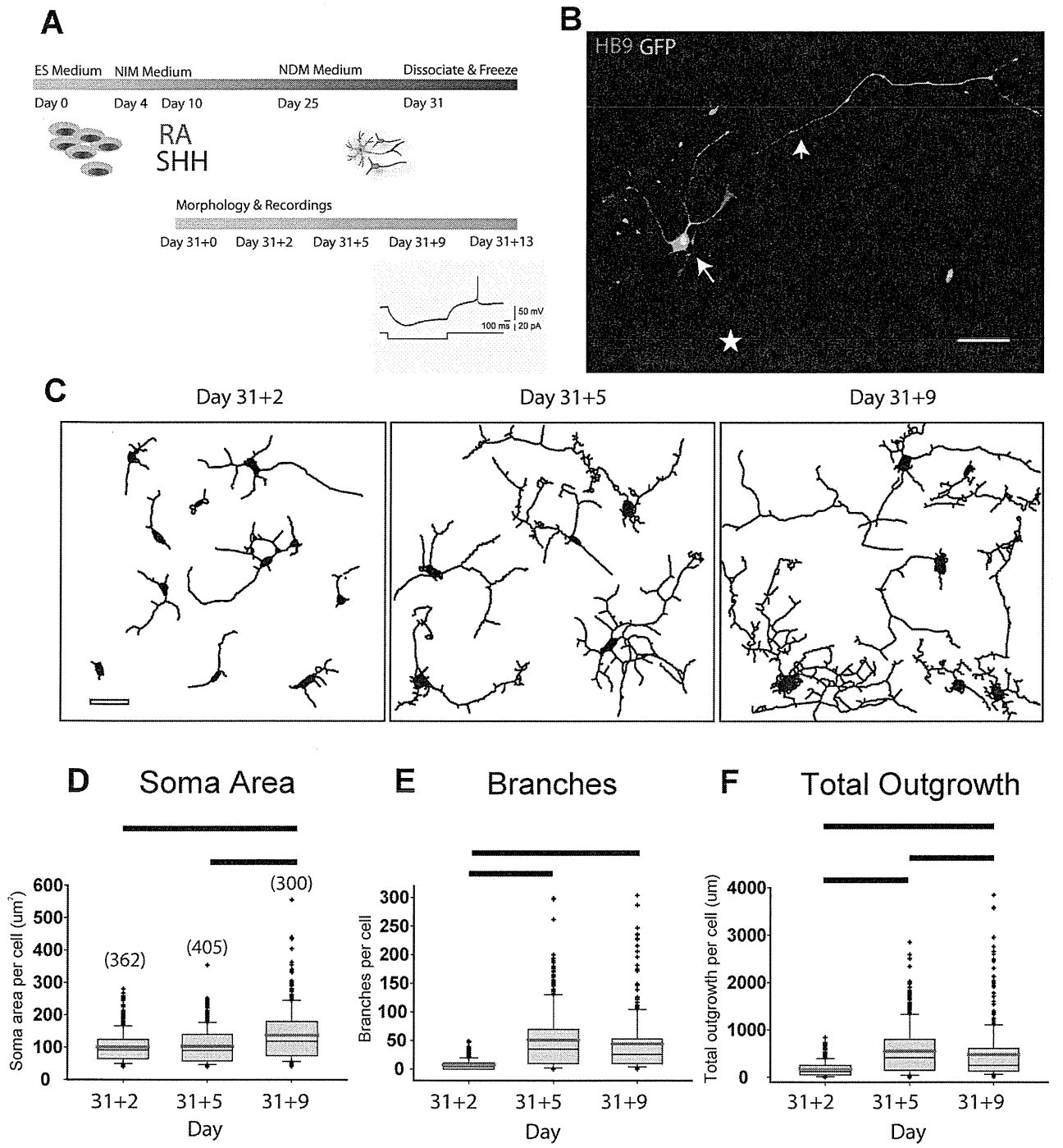

Figure 1. Human ES-derived motor neurons show increasing morphological complexity as they mature *in vitro*. (A) Top, schematic of ES cell directed differentiation to motor neurons shows timing of addition of the inductive cues retinoic acid (RA), and sonic hedgehog (SHH). Bottom, timing of morphometric and electrophysiological analyses. (B) Representative image of day 31+5 hESMN showing mature neuronal morphology and co-expression of GFP with motor neuron marker HB9. GFP intensity distinguished hESMN cell bodies (arrow, ~65,000 gray levels (g.l.)), neurites (arrowhead, ~18,000 g.l.), and cytoplasmic GFP background in non-MNs (star, ~800 g.l.). Scale bar 50 μm. (C) Representative camera lucida (Metamorph) neurite traces from 5 randomly chosen (every 8th) image fields at day 31+2, 31+5, and 31+9 show increasing neurite size and complexity. Scale bar 40 μm. (D-F) Soma area, branches, total neurite outgrowth and processes (not shown) were quantified (number of cells analyzed at each timepoint shown in brackets in D), median (grey line), mean (red line), 25–75 percentile (grey box), 10–90 percentiles (whisker bars), all outliers (+) are shown for each day from which measurements were made. The values for each morphometric parameter on each day were distributed non-normally (Shapiro-Wilk test, $P<0.05$) and Kruskal-Wallis One Way Analysis of Variance on Ranks showed significant changes in (D) cell soma area ($H=43.885$, 2 d.f., $P<0.001$), (E) complexity or branches/cell $H=309.245$, 2 d.f., $P<0.001$), (F) total neurite outgrowth ($H=161.287$, 2 d.f., $P<0.001$), and (not shown) number of primary neurites (median, 25th–75th percentile: day 33: 3, 2–5; day 36: 6, 5–9; day 40: 8, 6–12, $H=442.555$, 2 d.f., $P<0.001$). All significant *post hoc* pairwise comparisons, Dunn's Method, are shown by black bars on graphs. and all pairwise comparisons for primary neurite number were significant, $P<0.05$.

doi:10.1371/journal.pone.0040154.g001

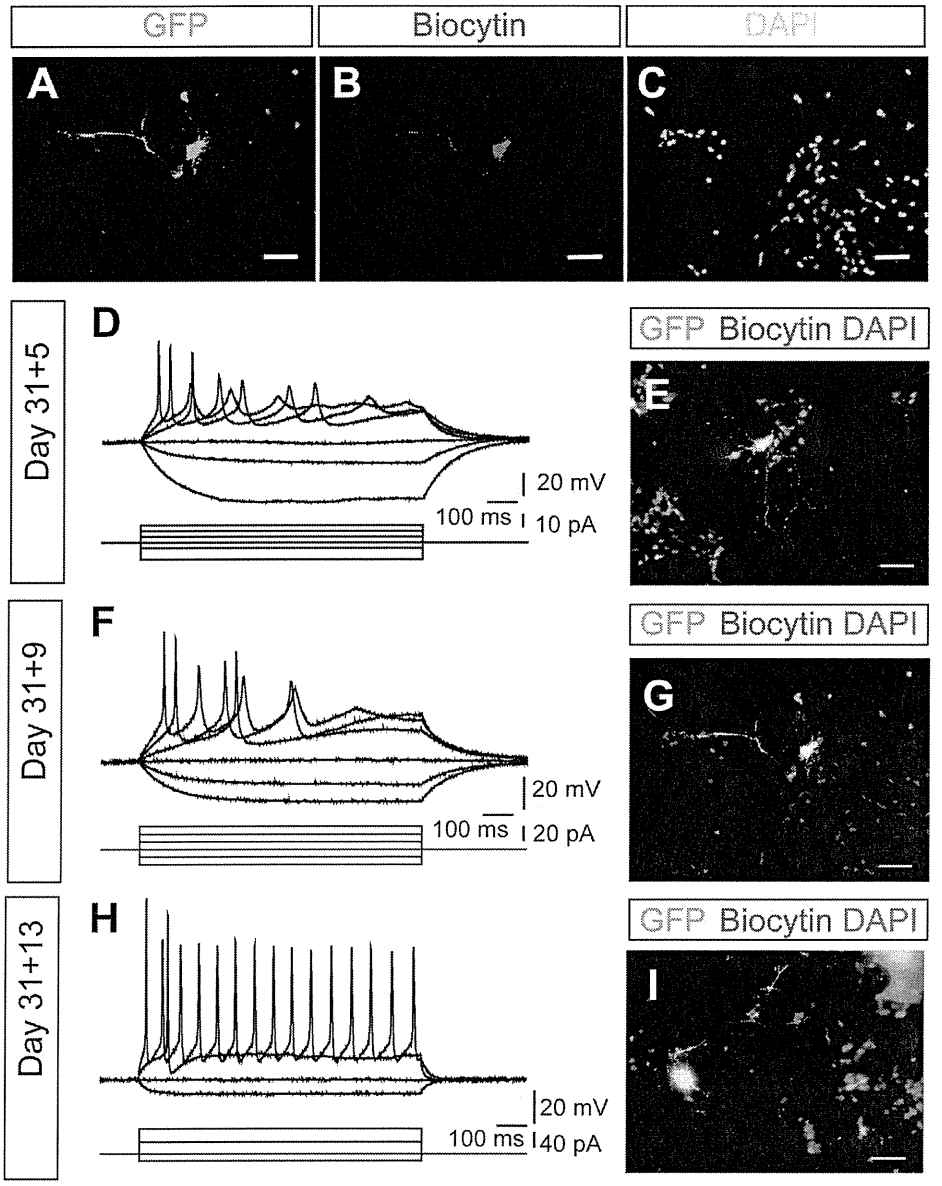

Figure 2. Representative morphology and membrane potential responses to current step injection in hESMNs at 3 different times *in vitro*. Imaging of cells fixed after patch-clamp recordings indicate that recorded cells express the *Hb9*::GFP reporter transgene (A-C,E,G,and I). Voltage responses and imaging in the same rows are taken from same neurons. The neurons for A-C are same as that shown in F and G. D,F,H show examples of voltage responses to current steps recorded from 3 neurons current-clamped at −58 mV, −60 mV, and −55 mV, respectively. Bottom traces in D,F, and H show injected currents. Scale bars in images are 50 μm.
doi:10.1371/journal.pone.0040154.g002

ages tested (31+12/31+13 DIV, 3 out of 9 neurons) still produced only a single action potential, even in response to a large depolarizing current step injection (>140 pA). Overall, however, these results suggest maturation in electrophysiological function of hESMNs with time in culture that is consistent with our morphological data.

Other Motor Neuron-like Electrophysiological Properties were Observed in hESMNs

In addition to repetitive firing, we investigated whether hESMNs have other physiological properties similar to motor neurons *in vivo*. Past reports showed a time-dependent decrease in action potential discharge rate during a sustained depolarization (increase in ISI) in spinal motor neurons or SFA [10,21,22,23,24]. Figure 4A shows an example of the change in instantaneous frequency measured throughout the repetitive firing response to a depolarizing stimulus. In general, instantaneous frequency drops throughout the train. To facilitate comparison of SFA at different ages, the SFA ratio was determined by calculating the ratio of ISI measured between the last two action potentials by ISI between the first two action potentials as illustrated in the inset of Figure 4A (and see Materials and Methods). SFAs increased with days *in vitro* (Fig. 4B, $n = 8$, $R = 0.73$, $P<0.05$, Pearson's linear regression), suggesting expression of conductances underlying SFA increased over the culture period.

In addition to SFA, we observed rebound depolarization after termination of hyperpolarizing current pulses in some hESMNs. These post-inhibitory rebound depolarizations sometimes reached

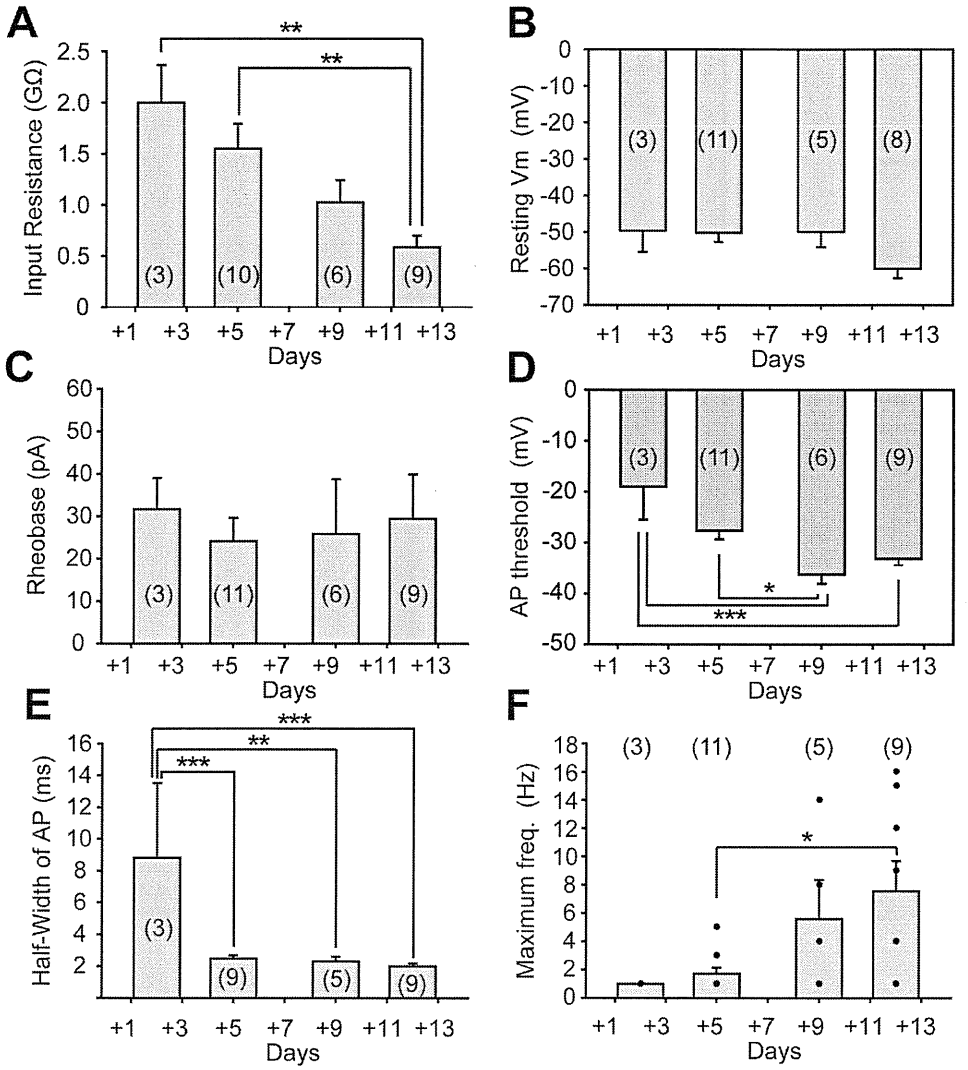

Figure 3. Developmental changes in intrinsic membrane properties of hESMNs. (A) Input resistance decreased over days *in vitro* (n = 28, P<0.01, one-way ANOVA). P<0.01, Tukey's *post hoc* test. (B) Resting membrane potential and (C) rheobase did not change (n = 27 and 29, respectively). Positive current steps were injected in 5 pA increments to distinguish small differences in rheobase among individual neurons. (D) Half-width of action potentials (APs),, changed over time *in vitro* (n = 26, P<0.001, one-way ANOVA). P<0.01, P<0.001, Tukey's *post hoc* test. (E) Maximum frequency of APs after current injection increased over time *in vitro* (n = 28, P<0.05, one-way ANOVA). P<0.05, Tukey's *post hoc* test. Dots shows frequency values for individual neurons. The numbers in parentheses indicate the number of neurons used for analysis taken from 22 dishes in total. In all panels, the first bar represents data from 31+2 DIV, 2nd bar is 31+4 DIV, 3rd bar is 31+8/31+9 DIV and 4th bar is 31+12/31+13 DIV.
doi:10.1371/journal.pone.0040154.g003

threshold for triggering an action potentials or RAPs, as shown in Figure 4C. In this study, none of the hESMNs tested at 31+2 DIV exhibited RAPs even after hyperpolarizations to ~−90 mV, although one of the neurons exhibited post-inhibitory rebound depolarization without reaching threshold for firing an action potential. However, 35 to 55% of hESMNs produced RAPs at 31+5 DIV and later (Fig. 4D). A similar age-dependent development of RAP has been observed in brainstem slices from rat hypoglossal motor neurons [15,25]. These results suggest that as hESMNs mature morphologically, they simultaneously acquire membrane properties similar to maturing motor neurons *in vivo*.

Rebound action potentials are due to post-inhibitory rebound depolarization and this depolarization has been shown to be due to activation of inward rectifier channels, low voltage activated Ca^{2+} channels, or both [17]. Inward rectification is evident in current clamp recordings as voltage sag back towards resting potential during a hyperpolarizing current injection (Fig. 4C). Five out of 26 neurons in our study met our criteria for sag (defined in Materials and Methods). All 5 of these neurons also had RAPs, suggesting the presence of sag could contribute to the depolarizing rebound and RAPs. Conversely, approximately half of the neurons with RAP had sag (5/12), suggesting the presence of sag was not required for RAPs.

Discussion

If hESMNs are to be useful for modeling human motor neuron development and function, it is important that they acquire mature functional characteristics similar to motor neurons *in vivo*. Here we provide evidence that hESMNs follow a time dependent course of maturation *in vitro* that can be measured by changes in morphology and electrophysiology. This maturation culminates in

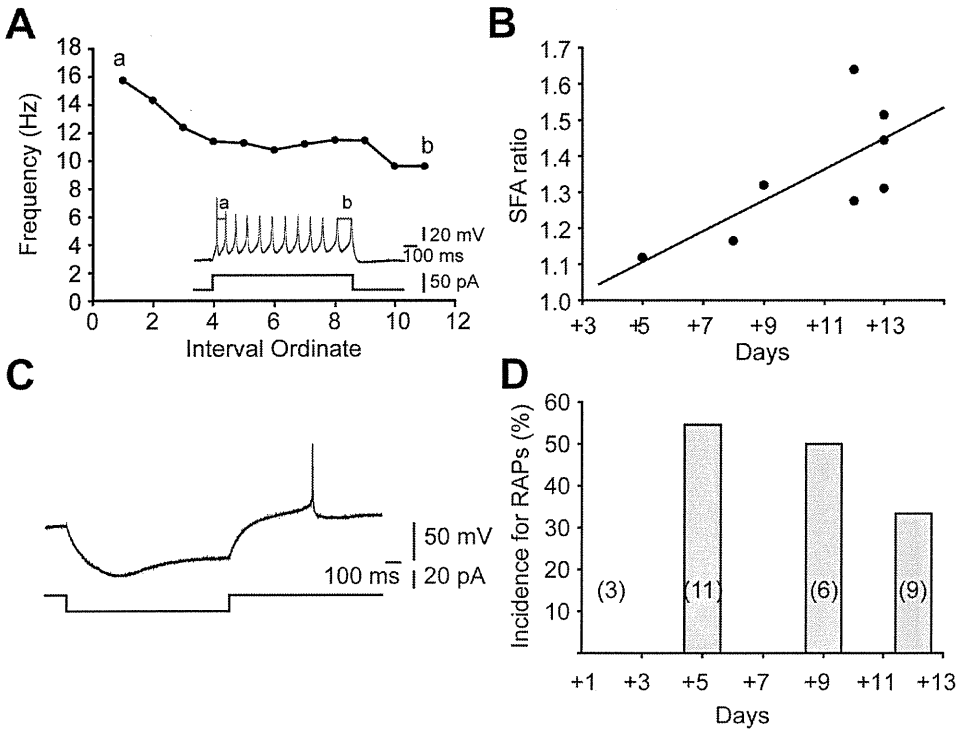

Figure 4. Spike frequency adaptation (SFA) and rebound action potentials (RAPs) in hESMNs. (A) An example of the change in instantaneous frequency during a train of action potentials evoked with positive current injection for 1 sec. Inset shows APs (upper) and injected currents (bottom). APs from which 'a' and 'b' ISI values were measure for SFA calculation are indicated. (B) SFA ratio, calculated as the maximum value of normalized ISIs after any amplitude of positive current injection, increased with DIV (n = 8, R = 0.73, P<0.05, Pearson's linear regression). (C) RAPs were observed in a large subset of hESMNs. Upper trace shows voltage change after negative current injection. Bottom trace shows injected negative current steps. RAP follows the return of current to baseline after the hyperpolarizing step. (D) Incidence of RAPs in hESMNs at 4 different ages as indicated in Fig. 3 legend (n = 29). Negative current steps with 5 pA increments (to at least 20 pA) were injected while checking for RAPs.
doi:10.1371/journal.pone.0040154.g004

functional physiological properties typical of maturing motor neurons *in vitro* and *in vivo*.

Developmental Changes in Morphology in hESMNs

Neuronal processes, including dendrites and axons, are essential elements in neural network connectivity. Mature mammalian spinal motor neurons have large cell bodies, long peripheral axons and extensive, long, branched dendrites that receive synaptic contacts across their entirety [26,27]. From day 31+2, 2 days after plating, to day 31+5 *in vitro*, hESMNs showed a rapid increase in neuritic outgrowth and branching (Fig. 1C,E, F). Neurite outgrowth continued to increase over the subsequent 4 days (Fig. 1F). In addition, a small but significant increase in soma area was observed towards the end of the *in vitro* observation period (Fig. 1C, D). By comparison, in mouse motor neurons *in vivo*, dendritic branching is maximal between embryonic day 13 (E13) and E15 at which time it starts to decrease. Rat and human motor neurons *in vivo* also show increases in number of processes and cell body size beginning gradually at rat E14, human gestational week 5.5, and have large cell bodies with typical multipolar morphology by rat E17, human gestational week 10.5 [6]. Mouse and rat motor neurons then show little change in complexity over the first two postnatal weeks [28,29]. The significant changes in hESMN morphology we have described, a steady increase in number of primary neurites, an increase in soma size, and an increase in total outgrowth, are consistent with the morphological changes embryonic rodent and human motor neurons display during development *in vivo*.

Developmental Changes in Membrane Properties Expressed in Maturing hESMNs

Intrinsic membrane properties of motor neurons change with maturation, including a more hyperpolarized resting membrane potential and decreased input resistance [5,7,8]. Similar changes have also been reported in developing motor neurons derived from mouse ES cells (mESMNs) [12,30]. In our studies, we have observed a decrease in input resistance but no change in resting potential. It is possible that we did not detect a change in membrane potential because we did not begin our recording until the second DIV. In studies with mESMNs, the greatest change in resting potential occurred over the first 2 DIV [12].

Physiological properties of developing rodent motor neurons change over the period of late embryonic development in a manner that is mirrored by hESMNs maturing in culture. At E15, rat motor neurons fire single action potentials with relatively long durations and shorter peak amplitudes relative to motor neurons in the postnatal rat [9]. Even E13 mouse spinal neurons grown in culture for less than 24 hours are able to fire single action potentials [31]. After birth, not only do action potentials recorded from rat motor neurons have a shorter duration and larger peak amplitude than embryonic motor neurons, they fire repetitively to a depolarizing current injection [9]. Similarly, mouse ES cell-derived motor neurons are able to fire repetitively by 3–4 DIV [12].

At early times *in vitro*, hESMNs showed several of the same characteristics as functionally immature, embryonic rodent motor neurons and mESMNs. They had single action potentials with

relatively long durations even after long lasting (1 s) large depolarizing current steps. By 31+8/31+9 and 31+12/31+13 DIV, hESMNs demonstrated the ability to fire a train of action potentials in response to a sustained depolarizing current step. The first action potential in the response had a significantly shorter duration than the single action potentials recorded from hESMNs at 31+2 DIV. Thus mature hESMNs acquired comparable electrophysiological properties to mature rodent motor neurons [10]. The mechanisms underlying the developmental changes in rat motor neurons observed neonatally and mESMNs include contributions from Na^+, K^+, and Ca dependent K^+ currents [9,12]. While we did not attempt to identify specific conductances responsible for these developmental changes in hESMNs, we can speculate that similar changes may be occurring.

hESMNs Appear to have Characteristic Active Membrane Properties of Motor Neurons

Motor neurons fire rhythmically during locomotion. Synaptic inputs onto motor neurons as well as intrinsic membrane properties of motor neurons contribute to this rhythm [32,33]. We have demonstrated two membrane properties in hESMNs that are induced by depolarizing and hyperpolarizing current pulses injection, SFA and RAP, respectively, that contribute to the firing pattern of motor neurons.

SFA in motor neurons is modulated by activity [14] and may contribute to efficient muscle contraction [13]. Repetitive stimulation of motor nerves was used to identify the pattern most optimal to produce efficient muscle contraction by Stein and Parmiggiani (1979). The optimal pattern consisted of a short first ISI followed by longer subsequent intervals, similar to the firing pattern that results from our depolarizing current pulses injection in hESMNs referred to as SFA (Fig. 4A, B). Slow inactivation of rapidly activating sodium channels has been shown to contribute importantly to SFA in mouse motor neurons [23]. Also consistent with increased expression and importance of sodium channels in hESMNs over DIV is the decrease in action potential half width together with the lack of change of rheobase and hyperpolarization of voltage threshold. In the face of strongly decreasing input resistance, all of these properties are consistent with an increased expression and density of fast sodium channels in hESMNs. Thus it is possible that these same sodium channels contribute to the increase in SFA with maturation of hESMNs that we have observed.

Rebound action potentials have been described in many neuronal systems. It is possible that activation of an inwardly rectifying current is the main cause of RAP in motor neurons [17], although other studies have suggested the contribution of low voltage-activated Ca^{2+} currents [7,34]. RAP may contribute to rhythmic activity of motor neurons during locomotion [7,17], suggesting that RAP is a hallmark of functional motor neurons. Some studies have demonstrated that RAPs contribute to shaping the pattern of neuronal firing. For example, observations of motor nerve function in Xenopus have shown that RAP plays a key role in the genesis of rhythmic motor pattern [35]. Experimentally induced RAP was able to initiate or modulate the bursting discharge of rat motor neurons during fictive locomotion [17]. In our studies, hESMNs showed this firing behavior characteristic of motor neurons in response to current pulses. Moreover, those characteristic behaviors in hESMNs were age-dependent (Figs. 4D) in that RAP was not apparent at 31+2 DIV whereas it was apparent at 31+5 to 31+13 DIV. These results support the idea that hESMNs progressively develop similar conductances to motor neurons *in vivo* that underpin their physiological function.

Variability in Morphological and Electrophysiological Properties of hESMNs

Our study revealed not only increasing maturity of electrophysiological and morphological properties of hESMNs over time in culture but also increasing variability of these parameters among the neurons tested at each time point. At least two mechanisms might contribute to this increasing variability. First, motor neuron birth is not synchronous in rodents or humans *in vivo* but follows a rostral to caudal progression (approximately embryonic day 30–50 in human) [6,36]. Analogous ongoing motor neuron neurogenesis *in vitro* might contribute to the variability of motor neuron functional characteristics as young, immature neurons are generated. Second, motor neurons at each spinal level are developmentally diversified into multiple subtypes [37,38], exhibiting diverse morphology and connectivity [39,40]. The variability of membrane properties we observed may reflect this variety of motor neuron subtypes. For example, it has been shown that back-labeled, embryonic chick motor neurons from the medial and lateral motor columns had significantly different input resistance and whole cell capacitance [41]. Deliberate specification of diverse motor neuron subtypes from stem cells has recently been demonstrated [42,43]. It will be interesting to determine in future experiments whether the diversity in electrophysiological and morphological properties observed *in vitro* can be attributed to molecularly defined populations of motor neurons.

Maturation of hESMNs *in vitro* followed a time course surprisingly similar to motor neuron maturation in late rodent embryonic development. As action potentials recorded from hESMNs themselves became faster and more robust, the pattern of firing mimicked that of newborn rodent motor neurons. While it is not possible to study human motor neuron maturation *in vivo* with this same resolution, hESMNs provide not only a model system in which function and development of human motor neurons can be studied, but also may provide a way to investigate human motor neuron diseases for which iPS-MNs are now becoming available.

Materials and Methods

Ethics Statement

The work performed in this paper on motor neurons derived from human embryonic stem cells has been approved by Columbia University ESCRO committee (Embryonic Stem Cell Research Oversight committee).

ESC Culture

A human embryonic stem cell line with a motor neuron reporter (BAC-*Hb9*::GFP) [19] was grown under standard pluripotency maintenance conditions: on irradiated CF-1 mouse embryonic fibroblast feeder cells (0.015 M cells/cm^2, GlobalStem) seeded on gelatinized (Millipore) tissue culture plastic. Cells were fed daily with ES Medium comprised of Dulbecco's Modified Eagle Medium: nutrient mixture F-12 (DMEM:F12, Invitrogen) with 20% Knockout Serum Replacer (Invitrogen), 110 μM beta-mercaptoethanol (BME; Sigma), L-Glutamine and Non Essential Amino Acids (NEAA; Invitrogen), and 20 ng/ml basic fibroblast growth factor (bFGF; Invitrogen) (ESC medium), and passaged weekly using 50 μg/ml dispase for 20 min (Invitrogen) followed by manual trituration. Parallel passages of ESCs were karyotyped at subsequent passages and found to be normal.

Motor Neuron Differentiation

After normal passage, washed ESC colonies were incubated for 1 hour in ESC medium, as described above, with 10 μM Rho-

associated kinase (ROCK) inhibitor (Y-27632, Ascent Scientific) [20], then trypsinized to single cells and seeded in suspension at 0.4 M cells/ml in ES medium with 10 μM ROCK inhibitor, and 300 ng/ml recombinant mouse Noggin (R&D). Fresh ROCK inhibitor, FGF, and Noggin were added daily for the first 6 days. Embryoid bodies (EBs) were pelleted at 100 G on day 4 and resuspended in DMEM F:12 plus N2 supplement (Invitrogen), NEAA, L-Glutamine, 2 μg/ml Heparin (Sigma), bFGF, Noggin, and ROCK inhibitor. EBs were pelleted and fed with fresh medium every other day until day 31. ROCK inhibitor was last added at day 5. Noggin and bFGF were discontinued at day 10, and 1:10 dilution of Wnt3a-L-cell conditioned medium (ATCC), all-trans retinoic acid (RA, 100 nM, Sigma), ascorbic acid (0.4 μg/ml, Sigma), db-cAMP (1 μM, Sigma), and recombinant mouse Sonic hedgehog (SHH) protein (100 ng/ml SHH-C25II, R&D) were added from day 10 onward. On Day 18 Wnt3a-conditioned medium was discontinued, SHH was increased to 200 ng/ml and recombinant human brain-derived neurotrophic factor (BDNF; 10 ng/ml, R&D) was added. At day 25, base medium was switched to Neurobasal with N2 and B27 (Invitrogen), L-Glutamine, NEAA, ascorbic acid, db-cAMP, (Neural Differentiation Medium (NDM)), with 10 ng/ml each recombinant human BDNF, glial cell-derived neurotrophic factor (GDNF), insulin-like growth faction 1 (IGF-1), and ciliary neurotropic factor (R&D), 200 ng/ml SHH, and 100 nM RA.

EBs were dissociated using trypsin on day 31 and cryopreserved using EmbryoMax 2× freezing medium (Millipore) for future use. Separate vials were thawed for electrophysiology and morphology time series, seeded on poly-ornithine/laminin coated glass coverslips, in complete day 25 NDM including all supplements. However, RA was reduced to 10 nM and SHH was reduced to 20 ng/ml and the following supplements were added: 1 μg/ml mouse laminin (Invitrogen), BME (25 μM, Sigma), glutamate (25 μM, Sigma), forskolin (20 μM, Sigma), and IBMX (100 μM, Fisher) at 250 K cells per 35 mm coverslip or 46 K cells per 15 mm coverslip. Half the medium was changed every 4 days.

Immunocytochemistry

Cultures were fixed for 30 minutes in 4% paraformaldehyde (PFA) in phosphate buffered saline (PBS) at 4°C, washed 3 times for 5 min in PBS, quenched and permeabilized in wash PBS plus 0.1% Triton X-100 (Wash buffer) plus 50 mM glycine for 15 min. Samples were blocked with Wash buffer plus 10% normal donkey serum for one hour, incubated with primary antibody in blocking buffer (chicken anti-GFP 1:1000, Invitrogen A10262; mouse anti-HB9,1:50, MNR2/815C10-s, Developmental Studies Hybridoma Bank) overnight. Cells were then washed, incubated with DyLight coupled donkey anti primary-species IgG antibodies (Jackson Immunoresearch, 1:1000). Finally, cells were washed and counterstained with DAPI (Invitrogen).

Imaging and Image Analysis

Coverslips were mounted in Fluoromount G and imaged on an inverted Zeiss AxioObserver Z1 using a 20× Plan-APOCHROMAT 0.8 NA objective and a 14-bit, gray scale Photometrics HQ2 CCD camera. Images were exported as 16 bit gray scale images for analysis. Cells were scored as $HB9^+$ or GFP^+ based on having >10 K mean gray levels of $HB9^-$ or >40 K mean gray levels of GFP-channel fluorescence intensity over local background, respectively, using the Metamorph Multiwavelength Cell Scoring module. Neurites were traced using the Neurite Outgrowth module (Metamorph) based on GFP fluorescence intensity of >3,000 g.l. over local background. A 20× field of view was manually adjusted to capture the maximum neurite outgrowth for each cell. This field size was sufficient to capture all neurites for almost all cells. At day 36 for example, the day at which the peak of total median outgrowth per cell occurs, less than 9% of GFP^+ cells had neurites extending beyond the field of view. Morphological measurements were grouped by days in culture and SigmaPlot11 was used for statistical analysis.

Electrophysiology

Whole-cell patch recordings were made from *Hb9*::GFP^+ motor neurons. Coverslips were transferred to the stage of a TE2000-E microscope (Nikon) and continuously perfused at a low flow rate of 1 ml/min with bath recording solution containing (in mM): 145 NaCl, 5 KCl, 2 $CaCl_2$, 10 HEPES, 2 $MgCl_2$ and 5.5 glucose, pH adjusted to 7.3 with NaOH, osmolality 325 mOsmol kg^{-1}. Patch pipettes with a resistance of 3–5 MΩ were pulled from borosilicate glass capillaries (0.86 mm ID, 1.5 mm OD) using a P-97 pipette puller (Sutter Instrument Co). Intracellular solution had the following composition (in mM): 120 potassium methanesulfonate, 10 NaCl, 10 EGTA, 1 $CaCl_2$, 10 HEPES, 0.5 NaGTP, 5 MgATP, 0.1% biocytin, pH adjusted to 7.2 with KOH, osmolality 280 mOsmol kg^{-1}. Some of the electrophysiologically recorded cells were filled with biocytin during recording, then were fixed, stained and imaged as above. Junction potential was corrected before recording.

Data were acquired using an Axopatch 200 B amplifier and pClamp 10 software (Molecular Devices, Sunnyvale, CA, USA). Data were filtered at 2 kHz and digitized at 20 kHz. Action potentials were evoked by injecting depolarizing currents of 1 s duration and analyzed using AxoGraph X software (AxoGraph Scientific, Sydney, Australia). Action potential characteristics in hESMNs were measured from resting membrane potential. The criterion for identification of a first action potential was when a voltage response to depolarizing current injection had obvious threshold, visible as a rapidly rising membrane potential that was positive to 0 mV. Rheobase was defined as the minimum current step amplitude required to evoke an action potential. Voltage threshold for action potentials was measured as in [44]. Action potential half-width was measured at rheobase. In a given cell, ISIs were calculated from recordings in which the maximum number of action potentials were evoked. Spike frequency adaptation (SFA) ratio was calculated as: ISI_{last}/ISI_{1st}. The calculation was performed only on data from neurons in which more than 5 action potentials could be evoked by a 1 s depolarizing current step. Sag was analyzed as the response following a hyperpolarizing current step that fit the following criteria: 1)The ratio between the size of voltage change at the steady state and the peak during a 1 sec current injection was greater than 1.1 and 2) the voltage change peaked during the first half of the current injection period.

Acknowledgments

We are grateful to Drs. Damian Williams and Lea Ziskind-Conhaim for helpful discussion and comments on an earlier version of the manuscript.

Author Contributions

Conceived and designed the experiments: TT GFC. Performed the experiments: TT GFC MWA. Analyzed the data: TT GFC MWA LS HW ABM. Contributed reagents/materials/analysis tools: LS. Wrote the paper: TT GFC MWA LS HW ABM.

References

1. Brownstone RM (2006) Beginning at the end: repetitive firing properties in the final common pathway. Prog Neurobiol 78: 156–172.
2. Lee H, Shamy GA, Elkabetz Y, Schofield CM, Harrsion NL, et al. (2007) Directed differentiation and transplantation of human embryonic stem cell-derived motoneurons. Stem Cells 25: 1931–1939.
3. Li XJ, Du ZW, Zarnowska ED, Pankratz M, Hansen LO, et al. (2005) Specification of motoneurons from human embryonic stem cells. Nat Biotechnol 23: 215–221.
4. Singh Roy N, Nakano T, Xuing L, Kang J, Nedergaard M, et al. (2005) Enhancer-specified GFP-based FACS purification of human spinal motor neurons from embryonic stem cells. Exp Neurol 196: 224–234.
5. Carrascal L, Nieto-Gonzalez JL, Cameron WE, Torres B, Nunez-Abades PA (2005) Changes during the postnatal development in physiological and anatomical characteristics of rat motoneurons studied in vitro. Brain Res Brain Res Rev 49: 377–387.
6. Altman J, Bayer SA (2001) Development of the human spinal cord: an interpretation based on experimental studies in animals. New York: Oxford University Press.
7. Martin-Caraballo M, Greer JJ (1999) Electrophysiological properties of rat phrenic motoneurons during perinatal development. J Neurophysiol 81: 1365–1378.
8. Ziskind-Conhaim L (1988) Electrical properties of motoneurons in the spinal cord of rat embryos. Dev Biol 128: 21–29.
9. Gao BX, Ziskind-Conhaim L (1998) Development of ionic currents underlying changes in action potential waveforms in rat spinal motoneurons. J Neurophysiol 80: 3047–3061.
10. Granit R, Kernell D, Shortess GK (1963) Quantitative Aspects of Repetitive Firing of Mammalian Motoneurones, Caused by Injected Currents. J Physiol 168: 911–931.
11. Meehan CF, Sukiasyan N, Zhang M, Nielsen JB, Hultborn H (2010) Intrinsic properties of mouse lumbar motoneurons revealed by intracellular recording in vivo. J Neurophysiol 103: 2599–2610.
12. Miles GB, Yohn DC, Wichterle H, Jessell TM, Rafuse VF, et al. (2004) Functional properties of motoneurons derived from mouse embryonic stem cells. J Neurosci 24: 7848–7858.
13. Stein RB, Parmiggiani F (1979) Optimal motor patterns for activating mammalian muscle. Brain Res 175: 372–376.
14. Brownstone RM, Krawitz S, Jordan LM (2011) Reversal of the late phase of spike frequency adaptation in cat spinal motoneurons during fictive locomotion. J Neurophysiol 105: 1045–1050.
15. Nunez-Abades PA, Spielmann JM, Barrionuevo G, Cameron WE (1993) In vitro electrophysiology of developing genioglossal motoneurons in the rat. J Neurophysiol 70: 1401–1411.
16. Viana F, Bayliss DA, Berger AJ (1993) Calcium conductances and their role in the firing behavior of neonatal rat hypoglossal motoneurons. J Neurophysiol 69: 2137–2149.
17. Bertrand S, Cazalets JR (1998) Postinhibitory rebound during locomotor-like activity in neonatal rat motoneurons in vitro. J Neurophysiol 79: 342–351.
18. Wichterle H, Lieberam I, Porter JA, Jessell TM (2002) Directed differentiation of embryonic stem cells into motor neurons. Cell 110: 385–397.
19. Placantonakis DG, Tomishima MJ, Lafaille F, Desbordes SC, Jia F, et al. (2009) Enriched motor neuron populations derived from bacterial artificial chromosome-transgenic human embryonic stem cells. Clin Neurosurg 56: 125–132.
20. Watanabe K, Ueno M, Kamiya D, Nishiyama A, Matsumura M, et al. (2007) A ROCK inhibitor permits survival of dissociated human embryonic stem cells. Nat Biotechnol 25: 681–686.
21. Gorman RB, McDonagh JC, Hornby TG, Reinking RM, Stuart DG (2005) Measurement and nature of firing rate adaptation in turtle spinal neurons. J Comp Physiol A Neuroethol Sens Neural Behav Physiol 191: 583–603.
22. Manuel M, Iglesias C, Donnet M, Leroy F, Heckman CJ, et al. (2009) Fast kinetics, high-frequency oscillations, and subprimary firing range in adult mouse spinal motoneurons. J Neurosci 29: 11246–11256.
23. Miles GB, Dai Y, Brownstone RM (2005) Mechanisms underlying the early phase of spike frequency adaptation in mouse spinal motoneurones. J Physiol 566: 519–532.
24. Powers RK, Sawczuk A, Musick JR, Binder MD (1999) Multiple mechanisms of spike-frequency adaptation in motoneurones. J Physiol Paris 93: 101–114.
25. Viana F, Bayliss DA, Berger AJ (1994) Postnatal changes in rat hypoglossal motoneuron membrane properties. Neuroscience 59: 131–148.
26. Burke RE, Glenn LL (1996) Horseradish peroxidase study of the spatial and electrotonic distribution of group Ia synapses on type-identified ankle extensor motoneurons in the cat. J Comp Neurol 372: 465–485.
27. Cullheim S, Fleshman JW, Glenn LL, Burke RE (1987) Membrane area and dendritic structure in type-identified triceps surae alpha motoneurons. J Comp Neurol 255: 68–81.
28. Li Y, Brewer D, Burke RE, Ascoli GA (2005) Developmental changes in spinal motoneuron dendrites in neonatal mice. J Comp Neurol 483: 304–317.
29. Nunez-Abades PA, Cameron WE (1995) Morphology of developing rat genioglossal motoneurons studied in vitro: relative changes in diameter and surface area of somata and dendrites. J Comp Neurol 353: 129–142.
30. Kuo JJ, Schonewille M, Siddique T, Schults AN, Fu R, et al. (2004) Hyperexcitability of cultured spinal motoneurons from presymptomatic ALS mice. J Neurophysiol 91: 571–575.
31. MacDermott AB, Westbrook GL (1986) Early development of voltage-dependent sodium currents in cultured mouse spinal cord neurons. Dev Biol 113: 317–326.
32. Hinckley CA, Hartley R, Wu L, Todd A, Ziskind-Conhaim L (2005) Locomotor-like rhythms in a genetically distinct cluster of interneurons in the mammalian spinal cord. J Neurophysiol 93: 1439–1449.
33. Rekling JC, Funk GD, Bayliss DA, Dong XW, Feldman JL (2000) Synaptic control of motoneuronal excitability. Physiol Rev 80: 767–852.
34. Martin-Caraballo M, Greer JJ (2001) Voltage-sensitive calcium currents and their role in regulating phrenic motoneuron electrical excitability during the perinatal period. J Neurobiol 46: 231–248.
35. Roberts A, Tunstall MJ (1990) Mutual Re-excitation with Post-Inhibitory Rebound: A Simulation Study on the Mechanisms for Locomotor Rhythm Generation in the Spinal Cord of Xenopus Embryos. Eur J Neurosci 2: 11–23.
36. Nornes HO, Das GD (1974) Temporal pattern of neurogenesis in spinal cord of rat. I. An autoradiographic study–time and sites of origin and migration and settling patterns of neuroblasts. Brain Res 73: 121–138.
37. Dalla Torre di Sanguinetto SA, Dasen JS, Arber S (2008) Transcriptional mechanisms controlling motor neuron diversity and connectivity. Curr Opin Neurobiol 18: 36–43.
38. Dasen JS, Jessell TM (2009) Hox networks and the origins of motor neuron diversity. Curr Top Dev Biol 88: 169–200.
39. Cameron WE, Averill DB, Berger AJ (1985) Quantitative analysis of the dendrites of cat phrenic motoneurons stained intracellularly with horseradish peroxidase. J Comp Neurol 231: 91–101.
40. Rose PK, Keirstead SA, Vanner SJ (1985) A quantitative analysis of the geometry of cat motoneurons innervating neck and shoulder muscles. J Comp Neurol 239: 89–107.
41. Soundararajan P, Miles GB, Rubin LL, Brownstone RM, Rafuse VF (2006) Motoneurons derived from embryonic stem cells express transcription factors and develop phenotypes characteristic of medial motor column neurons. J Neurosci 26: 3256–3268.
42. Peljto M, Dasen JS, Mazzoni EO, Jessell TM, Wichterle H (2010) Functional diversity of ESC-derived motor neuron subtypes revealed through intraspinal transplantation. Cell Stem Cell 7: 355–366.
43. Patani R, Hollins AJ, Wishart TM, Puddifoot CA, Alvarez S, et al. (2011) Retinoid-independent motor neurogenesis from human embryonic stem cells reveals a medial columnar ground state. Nat Commun 2: 214.
44. Takazawa T, Saito Y, Tsuzuki K, Ozawa S (2004) Membrane and firing properties of glutamatergic and GABAergic neurons in the rat medial vestibular nucleus. J Neurophysiol 92: 3106–3120.